PROCESSING AND FEATURE EXTRACTION OF BIOMEDICAL IMAGES

A DISSERTATION

Submitted in partial fulfillment of the requirements for the award of the degree of

MASTER OF TECHNOLOGY

in

ELECTRICAL ENGINEERING

(With Specialization in System Engineering and Operations Research)

By

Y.VIVEKANAND

DEPARTMENT OF ELECTRICAL ENGINEERING
INDIAN INSTITUTE OF TECHNOLOGY ROORKEE
ROORKEE-247 667 (INDIA)

JUNE, 2006

ID No. MT-352|2006-47|YV-HOG-VK.

CANDIDATE'S DECLARATION

I here by declare that the work which is being presented in this dissertation entitled **"PROCESSING AND FEATURE EXTRACTION OF BIO-MEDICAL IMAGES"** in partial fulfillment of the requirement for the award of the degree of **Master of Technology** in **Electrical Engineering**, submitted in the Department of Electrical Engineering of the Indian Institute of Technology Roorkee, Roorkee, is an authentic record of my work carried out for a period from July 2005 to June 2006, under the supervision and guidance of **Dr. H. O. Gupta** and **Dr. Vinod Kumar**

The matter embodied in this dissertation has not been submitted by me for the award of any other degree.

Date: June 29, 2006
Place: Roorkee

Y. vivekanand
Y.VIVEKANAND

CERTIFICATE

This is to certify that the above statement made by the candidate is correct to the best of my knowledge.

Dr. H.O.GUPTA
Professor, Electrical Engg.
Indian Institute of Technology Roorkee
Roorkee-247667, India

Dr. VINOD KUMAR
Professor, Electrical Engg.
Indian Institute of Technology Roorkee
Roorkee-247667, India

ACKNOWLEDGEMENT

I take this opportunity of expressing my deep sense of gratitude and indebtedness to my guide **Dr.H.O.Gupta,** Professor, Electrical engineering department, IIT Roorkee, for his invaluable help and encouragement. Without his good self and support, it would not have been possible for me to complete the thesis. I am glad to mark that it is a great experience for me to learn under his guidance.

I would like to thank my co-guide **Dr.Vinod Kumar,** Professor, Electrical engineering department, IIT Roorkee, for his exceptional supervision & guidance throughout the entire duration of the thesis study, whose suggestions formed a great asset to me. It is through significant discussions with them that this thesis evolved and took a complete form.

I appreciate the assistance and quick-response help from the professionals of System Engineering and Operations Research group.

I am grateful for the constant support, love and encouragement from my family and friends that helped me to carry on my work and present it effectively.

Dated: June 29, 2006

Place: Roorkee

Y.Vivekanand

Y.VIVEKANAND

ABSTRACT

Processing of Bio-Medical Images, extracting the features and obtaining other important information from them are the latest trends in the disease diagnosis. Digital Mammography is the recent tool in the field of Breast Cancer diagnosis. As the conventional clinical ways of processing and feature extraction is quite cumbersome and error prone for the Radiologists, computer aided processing and extraction of features from them becomes a better option to relay on, in the process of detection of the disease.

Two important problems that have been covered in this thesis with regarding to digital mammography are Enhancement of the mammographic images and the second one is detection of subtle and complex microcalcifications, which are an important symptom of breast cancer.

A detailed computational procedure has been developed for the quantitative comparison of different enhancement techniques for the digital mammograms. This procedure will gives out the best enhancement technique based on recently proposed quantitative measures. Multiscale decomposition of mammograms based on Multiresolution Analysis using wavelets has been carried out, which helps in detecting the microcalcifications. Wavelet analysis is an extremely powerful data representation method that allows for the separation of images into different frequency bands without affecting the spatial locality. Thus, information concerning localized high-frequency signals such as microcalcifications can be extracted effectively.

CONTENTS

LIST OF FIGURES

INTRODUCTION

This dissertation deals with processing and extracting the features from the digital mammograms. This introduction outlines the applications context and motivates the importance of the problem.

1.1 Motivation

Breast cancer is by far the most common cancer among women. Although lung cancer has a lower incidence (fewer diagnosed cases) than breast cancer, more women die each year of lung cancer. However, the majority of deaths from lung cancer can be attributed to smoking, and so breast cancer continues to be the leading cause of non- preventable cancer death. Additionally, the etiologies of malignant breast cancer are unclear, and no single dominant cause has emerged. According to the International Agency for Research on Cancer, more than one million women suffer from this type of cancer and more than 0.4 million deaths have occurred because of this type of cancer [1]. In India about 2.0 to 2.5 million patients suffer from cancer at any given time. According to the National Cancer registry program, breast cancer has replaced the cervix as the leading site of cancer in all urban population based cancer registries [2].

Although there is currently no known way of preventing breast cancer, researchers established that the key to breast cancer survival rests upon its earliest possible detection. Currently, Digital mammography is the single most important factor in early detection, and screening mammography could result in at least a percent reduction in breast cancer deaths.

1.2 Screening Mammography

A screening mammography program separates normal mammograms from the abnormal ones. The abnormal mammograms are then further evaluated by methods such as diagnostic mammography or biopsy to determine if a malignancy exists. A standard mammogram screening case consists of four images, two views of each breast. There is a cranio-caudual (CC) or top-to-bottom view, and a medio-lateral

(ML) or Middle-to-outside view. Each image is an X-ray image. The high/bright values in the image, by common convention, represent high absorption of X-rays. Conversely, the low/dark values represent low absorption of X-rays. Sometimes an abnormality (or "suspicious region") will be missed by a radiologist or imperceptible in one view, but easily detected in the other view. Here is a typical digital mammogram has been shown.

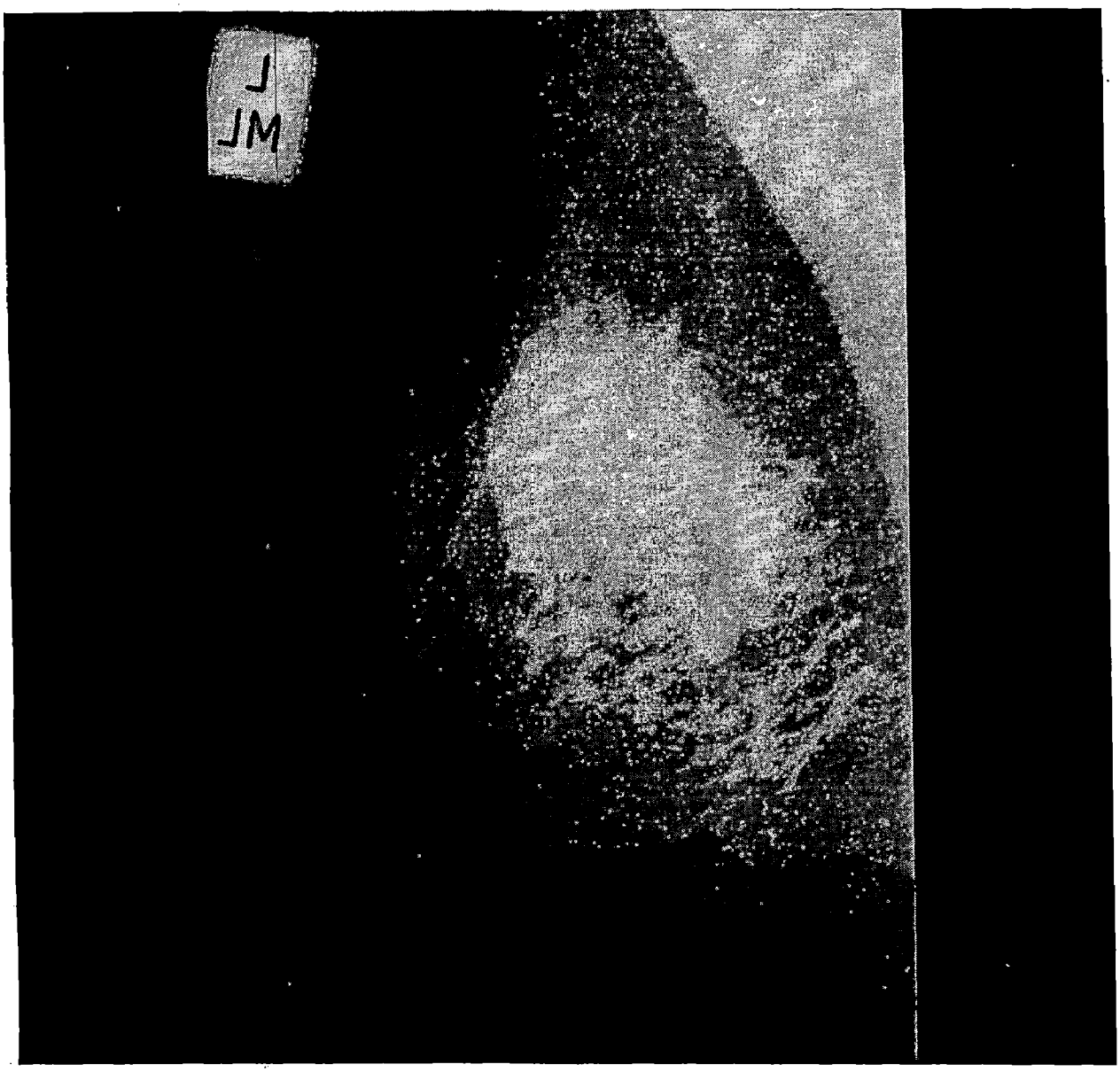

Fig.1.1 A typical Mammogram. Courtesy Mini MIAS, file name: mdb209.pgm [8]

1.2.1 Mammographic Abnormalities

A radiologist looks for certain signs and characteristics indicative of cancer when evaluating a mammogram. Among these signs are the presence of clustered microcalcications (or just "calcifications"), spiculated (or stellate) lesions, circumscribed (or well defied masses), ill-defied (or "irregular") masses, and architectural distortions. Asymmetry and developing densities are also important.

Unfortunately, mammograms are among the most difficult of radiological images to interpret, in particular, microcalcification visual assessment turns out to be an actual challenging task. A microcalcication is a tiny calcium deposit that has accumulated in the tissue in the breast, and it appears as a small bright spot on the mammogram. A cluster is typically defined to be at least 2 to 5 microcalcications within a square centimeter region. The calcications vary in size from smaller than 0.1 millimeter to 1 millimeter in diameter [6], and a radiologist must carefully examine the mammogram with a magnifier to locate calcifications which may be embedded in dense tissue. Size, shape, and radiographic density are the most important factors when analyzing individual calcifications. The number and distribution of calcifications within a cluster are also considered [3].

1.3 Computer Analysis

Computer aided diagnosis (CAD) and automated prescreening by computer are two ways to potentially counter many of the problems that would result from screening a large number of women for breast cancer using mammography. In a CAD scenario, computerized image analysis is used to suggest possible suspicious regions in the image so that the radiologist can then examine these regions more carefully. Additionally, image processing operations, such as contrast enhancement and edge detection, can be applied to the image at the request of the human reader before a decision is made. The automated prompting and the additional information provided by computerized image analysis should result in greater repeatability and uniformity in the standard of care. It should also result in some increase in sensitivity for a given level of specificity: that is, more cancers detected (fewer missed cancers) with the same biopsy rate. The cancers detected as a result of the increased sensitivity would then be treated earlier and thus less expensively and with a higher cure rate. Indeed,

evidence is mounting that prompting the radiologist with computer detection results of mammogram images leads to an increased sensitivity without affecting specificity.

In a CAD scenario, the computer essentially acts as a second reader without incurring the cost of an additional radiologist. In institutions in which double reading is the current practice, the computer could become one of the readers. There is effectively more physician time available, and an increased number of studies could be examined without an increase in cost. When standard practice is for a single radiologist to read each case, the average time spent reading each mammogram may or may not increase. However, a slight increase in average time per mammogram, if that is the case, would be reasonable since the radiologist is considering more information when making a decision. Since this extra information can help achieve a better sensitivity/specificity tradeoff, the extra time spent could possibly be justified in a cost-effectiveness sense. A computerized search of a mammographic image for abnormalities is systematic and complete. Digital mammography is identified as an evolving technology with the greatest potential impact on management of breast cancer. Indeed there are numerous research groups and funding agencies around the world that are actively pursuing research in digital mammography and computerized mammogram image analysis.

1.4 Thesis Overview

The work in this dissertation concentrates on two main aspects of digital mammography: one is enhancement of mammographic images to achieve better visibility of the observed phenomena to the human observer (radiologist), and processing of mammograms to enable automatic detection of micro-calcifications, as a first step to the "automated second-opinion" procedure.

Image enhancement or pre-processing step of mammograms refers to attenuation, or sharpening of image features such as edges, boundaries, or contrast to make the processed image more useful for analysis. Image enhancement includes gray level and contrast manipulation, noise reduction, background removal, edge crisping and sharpening, filtering, and so on.

Multi-scale methods based on wavelet transform have been applied on the mammographic images, so that microcalcification detection is directly accomplished within the transform domain, and the threshold is experimentally chosen as a fixed percentile of the histogram of each channel.

1.5 Organization of the Report

This report focuses on processing and detecting microcalcifications from the digital mammograms. Rest of the report is organized as follows,

Chapter 2 focuses on the literature review. It is organized into chronological order, which provides previous work and the recent contributions.

Pre-processing of the X-ray mammograms, so that they can be converted into Digital Mammograms, and various processing operations on Digital Mammograms like cropping of ROI, enhancing techniques are discussed in the 3 rd chapter.

The need of the evaluation techniques of enhancement techniques and recently proposed different enhancement techniques have been discussed in chapter 4.

Various Transformation based techniques for the detection of calcifications, and their chronological development is given in the chapter 5. And this chapter tries to answer the question: why the researchers shifted their attention to the wavelet analysis?

Chapter 6 explains in detail about the Multi Resolution Analysis, which is the crucial part in detecting the microcalcifications from the digital mammograms.

The Results obtained at different stages of the work and the conclusions that are drawn from them are discussed elaborately in the 7th chapter.

LITERATURE REVIEW

Though there is a lot of research work is going on in the field of processing and extracting features from digital mammograms, still there is no universal method is evolved in processing them and finding the microcalcifications. Here some of the previous work that has been done in the field of digital mammogram processing and feature extraction has been given.

2.1 Previous work

The fundamental enhancement needed in mammography is an increase in contrast, especially for dense breasts. Contrast between malignant tissue and normal dense tissue may be present on a mammogram but below the threshold of human perception. Similarly, microcalcifications in a sufficiently dense mass may not be readily visible because of low contrast [20].

Conventional image processing techniques do not perform well on mammographic images. The large variation in feature size and shape reduces the effectiveness of classical fixed neighborhood techniques such as unsharp masking [18]. Morrow *et al.* [18] used a "region-based image processing" technique which adapts to image features and enhances these features with respect to their surroundings, regardless of the shape and size.

Ted C. Wang *et al.* proposes two possible approaches to enhancing mammographic features. One is to increase the contrast of suspicious areas as stated earlier, and the other is to remove background noise [10].

Kim *et al.* proposes a local adaptive enhancement technique which increases the contrast rate in similar contrast region like in mammograms, and decreases the contrast rate in high contrast region [11].

Indeed, computer-aided analysis of microcalcifications in digital mammograms is widely reputed as a remarkable goal, and several methods have been proposed in the literature for their detection and segmentation. The effectiveness of such techniques can be assessed taking into account True Positive (TP) and False Positive (FP) detections[12]. FP is the probability of incorrectly classifying a non target object as a target object - the microcalcification - while TP detection rate is the probability of correctly classifying a target object.

One of the early methods achieving significant clinical results is that of Davies and Dance [13], with experiments performed over 50 test images, half of which contained no clusters. The authors report a 96% TP with an average of 0.18 FP clusters per image. However, the authors detect suspicious areas by using a local threshold and, to such end, the selected regions are limited by size criteria; further, those with an irregular shape are discarded.

The method due to Dengler *et al.* [14] exploits a two-stage algorithm for spot detection and shape extraction, based on Gaussian filter detection followed by morphological reconstruction. They report 70% of TP and 0.3 FP. Such a result is tested using a number of mammograms evaluated through the judgments of expert radiologists, although the mammographies are not publicly available and the outcome cannot be compared with other methods.

Shen et al. [4] propose a multi-tolerance region growing method. The resulting regions are then given in input to a neural network for classification. The results are the following: in mammograms containing benignant tumors, they achieve 81% of TP and zero FP, while 85% TP and 29 FP of malignant cases are reported. It has to be noted that the experiments, albeit biopsy proved, have been performed on a very low number of images, four real mammograms, that are not publicly available.

2.2 Recent Contributions

Sameer Singh et al [23-24] proposes a novel set of metrics that measure the quality of the image enhancement of mammographic images in a computer-aided detection framework aimed at automatically finding masses using machine learning techniques. Their methodology includes a novel mechanism for the combination of the metrics proposed into a single quantitative measure.

Multiresolution methods, such as the use of the wavelet transform, originally developed in the signal processing field [19] have recently been proposed for image enhancement, segmentation and edge detection in the field of digital mammography [15].Multiresolution approaches have an inherent advantage over traditional filtering methods, which primarily focus on the coupling between image pixels on a single scale and generally fail to preserve image details of important clinical features.

The motivations for adopting an image multi-scale representation ground in the wealth of physiological and psychophysical data demonstrating that the visual system analyzes images at different resolutions: visual information is processed in parallel by a number of spatial-frequency –tuned channels and in the visual pathway, filters of different size operate at the same location[3].

. Recently, a variety of schemes for the computerized detection of microcalcification based on wavelet transform have been proposed [4]-[5].In these schemes, the mammogram image is passed through a sub-band decomposing filter bank. The sub-band images are weighted to enhance the microcalcification locations, and the new image is reconstructed from the weighted sub-image. The detection method using the global and gray level threshold is applied to the reconstructed images. In particular, Strickland's approach [6] is appealing as regards both the results achieved and the methodology. Microcalcification detection is directly accomplished within in the transform domain, relying on a thresholding of the wavelet coefficients to produce a detect/no detect result.

PROCESSING OF MAMMOGRAPHIC IMAGES

As the X-ray Mammograms can not be processed directly by a computer, they should be converted into Digital form. Various Processing techniques like cropping and enhancement are carried out on digital mammograms have been discussed in this chapter.

3.1 Pre-Processing of Mammograms

The X-ray mammographic images have to be digitized in order to process them on a computer. In standard mammography, images are recorded on film using an x-ray cassette. The film is viewed by the radiologist using a "light box" and then stored in a jacket in the facility's archives. With digital mammography, the breast image is captured using a special electronic x-ray detector, which converts the image into a digital picture for review on a computer monitor. The digital mammogram is then stored on a computer. With digital mammography, the magnification, orientation, brightness, and contrast of the image may be altered after the exam is completed to help the radiologist more clearly see certain areas.

In this dissertation work, the Mammographic Image Analysis Society (MIAS) Mini Mammographic Database [8], which contains 322 mammograms including normal, mass, and microcalcification cases, have been used. The image size in the Mini Mammographic database has been clipped and padded to become 1024×1024 pixels whose spatial resolution is 200μm and dynamic range is 8-bit. In this work, the microcalcifications of 0.05 to 1.0 mm in diameter are of interest, which corresponding to one to five pixels in diameter.

3.2 Cropping of Mammograms

Mammograms, in general have a lot of background masses and other details, which makes it difficult in the process detection of microcalcifications. So it is a good idea that cropping the suspected regions in the mammogram, which are specified by the radiologist. Instead of processing the entire mammogram, it is easier to process the segmented region. Here, as an example is shown, this gives the details of cropping of the mammogram.

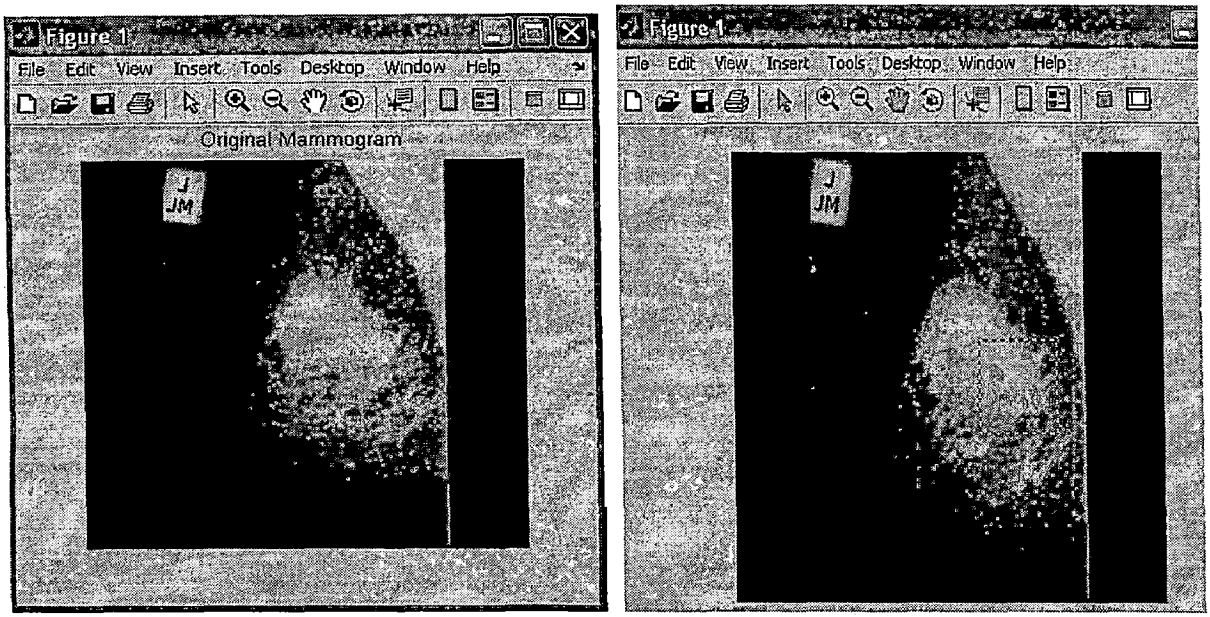

(a) (b)

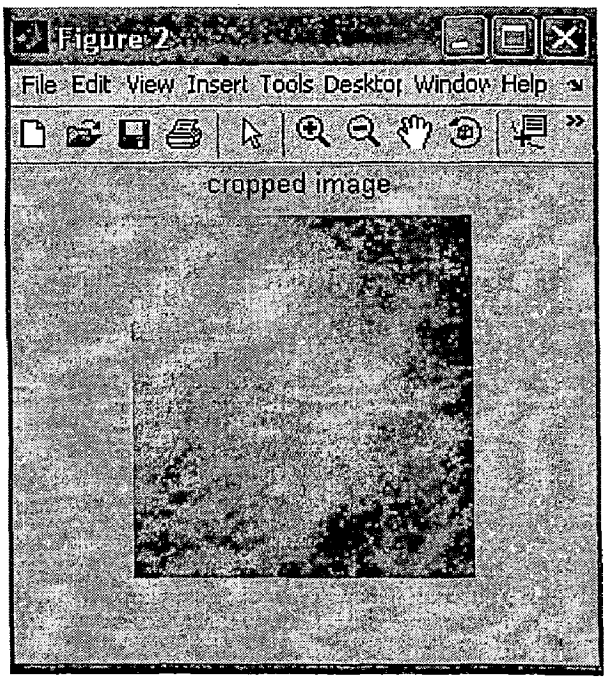

(c)

(a) Original Mammogram (mdb249)

(b) Snapshot of Cropping

(c) Cropped Image.

Fig. 3.1 Cropping of Mammogram

3.3 Enhancement of Mammograms

Image Enhancement refers to attenuation, or sharpening of image features such as edges, boundaries, or contrast to make the processed image more useful for analysis. Image enhancement includes gray level and contrast manipulation, noise reduction, background removal, edge crisping and sharpening, filtering, and so on. In the following, we summarize some enhancement techniques for mammographic images used in this work. The processing step consists of two main techniques that are used individually or together. The first technique deals with the contrast enhancement of suspicious areas in the mammographic image while the second technique involves the removal of background noise from the image.

3.3.1 Enhancement by Direct Contrast Stretching

Low-contrast images occur often due to poor or non-uniform lighting conditions or due to nonlinearity or small dynamic range of the imaging sensors. In the case of mammograms most of the images having their dynamic range confined to a small band of gray scale.

The direct contrast enhancement is based on the local contrast measure associated to each pixel and its contrast enhancement function. The original values of gray level are expanded into full gray scale, depends upon the class of the image, i.e., whether the image is double or uint8 or uint16. The output enhanced value, . (x, y), of the direct contrast enhancement is also follows, and A(x, y) are the gray value of each pixel in the original image, respectively [9].

$$O(x,y) = (A(x,y) - A(x,y)_{min}/(A(x,y)_{max} - A(x,y)_{min}))$$

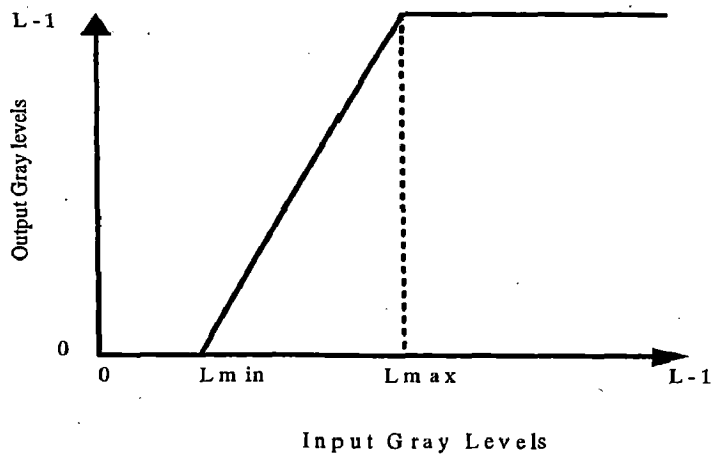

. **Fig.3.2** Graphical representation of Contrast Stretching

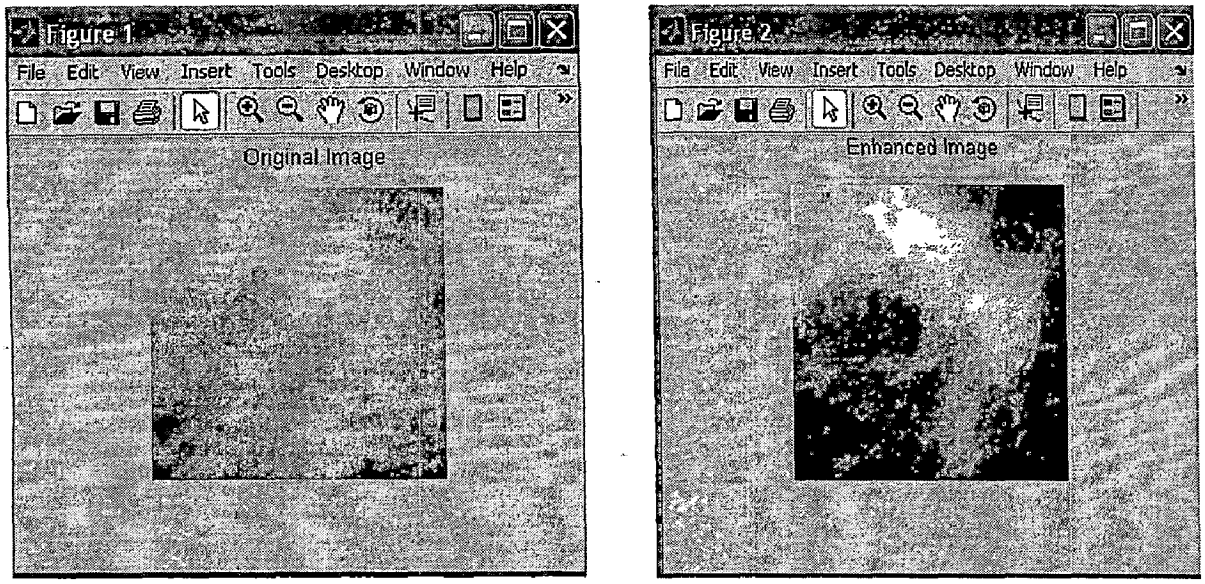

(a) Original Image (b) Enhanced Image

Fig.3.3 Enhancement by Contrast Stretching

3.3.2 Enhancement by Histogram Equalization

Histogram Equalization is a very famous technique, which is used to improve the contrast of the image. The histogram of a digital image with gray levels in the range with gray levels in the range [0, L-1] is a discrete function $h(r_k) = n_k$, where r_k is the *k*th gray level and n_k is the number of pixels in the image having gray levels r_k. it is common practice to normalize a histogram by dividing each of its values by the total number of pixels in the image, denoted by *n*. thus, a normalized histogram is given by $p(r_k) = n_k/n$,

for $k = 0,1,2,..L-1$. Loosely speaking $p(r_k)$ gives an estimate of the probability of occurrence of gray level r_k. Note that the sum of all components of a normalized histogram is equal to 1.

We note that in the dark image that the components of the histogram are concentrated on the low (dark) side of the gray scale. Similarly, the components of the histogram of the bright image are biased toward the high side of the gray scale. An image with low contrast has a histogram that will be narrow and will be centered toward the middle of the gray scale. And the components of the histogram in the high-contrast image cover a broad range of the gray scale and, further, that the distribution of pixels is not too far from uniform, with very few vertical lines being much higher than the others. Intuitively, it is reasonable to conclude that an image, whose pixels

tend to occupy the entire range of possible gray levels and, in addition, tend to be distributed uniformly, will have an appearance of high contrast and will exhibit a large variety of gray tones.

Here an example is shown, which describes the histogram equalization of the mammogram.

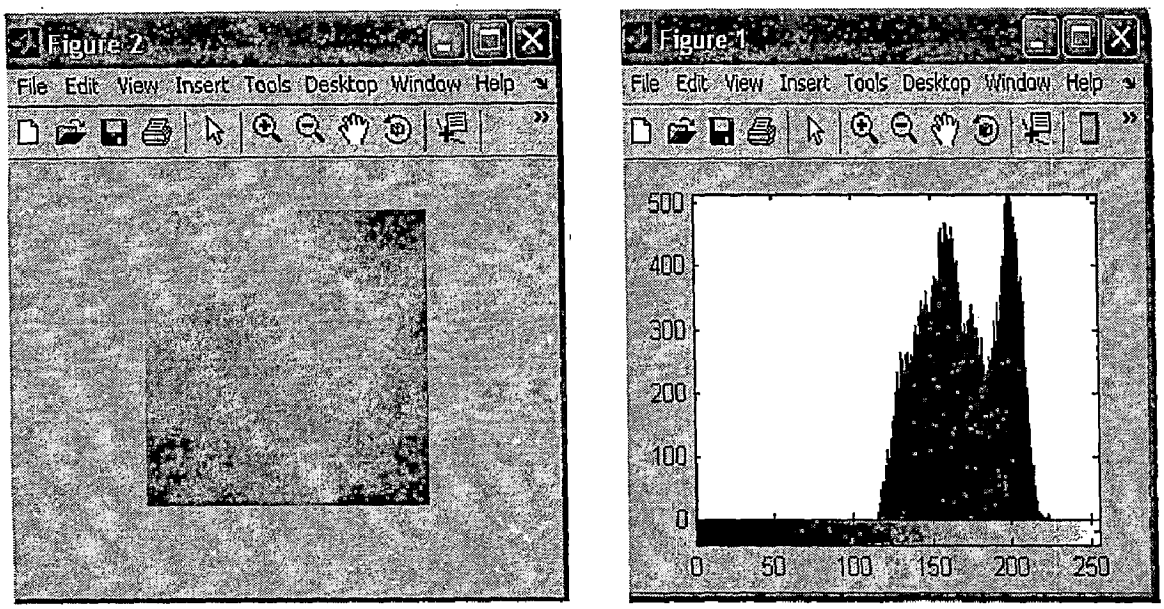

(a) Original ROI Image (b) Histogram of (a)

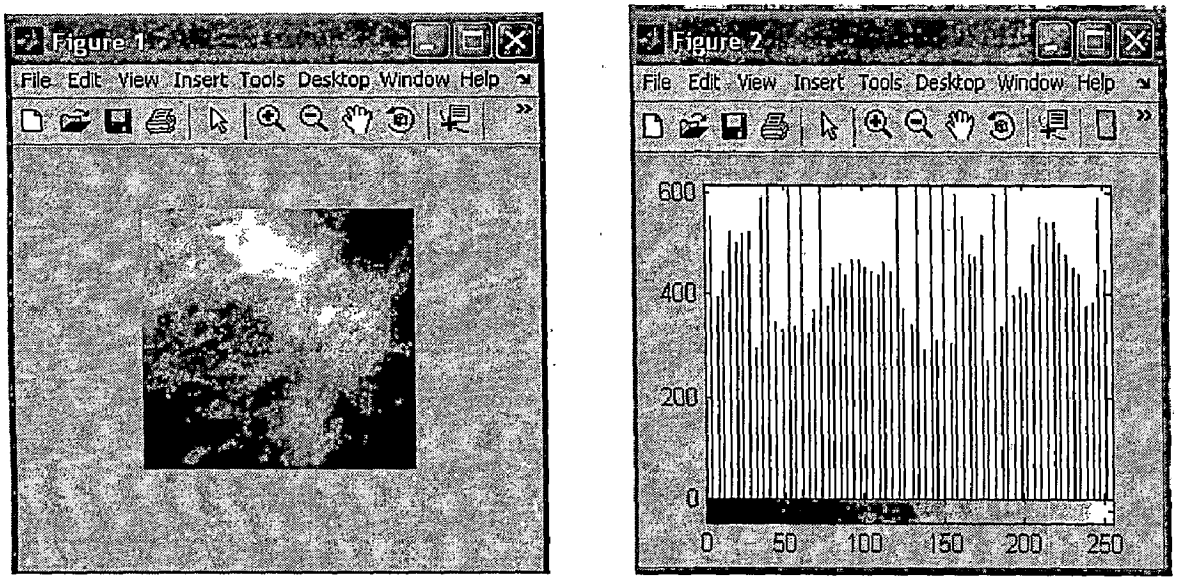

(c) Enhanced image (d) Histogram of (c)

Fig. 3.4 Enhancement of ROI of 'mdb209' by Histogram Equalization

3.3.3 Contrast Limited Adaptive Histogram Equalization

In contrast to the Histogram Equalization, which evenly distributes the entire image pixels over the dynamic range, Contrast Limited Adaptive Histogram Equalization (CLAHE), it operates on small data regions (tiles), rather than the entire image.

The entire image is subdivided into number of data regions (tiles), and then histogram equalization is applied on each tile of the image. Each tile is enhanced, so that the output is approximately matches the specified histogram (default is uniform distribution). The contrast, especially in homogeneous areas, can be limited in order to avoid amplifying the noise which might be present in the image.

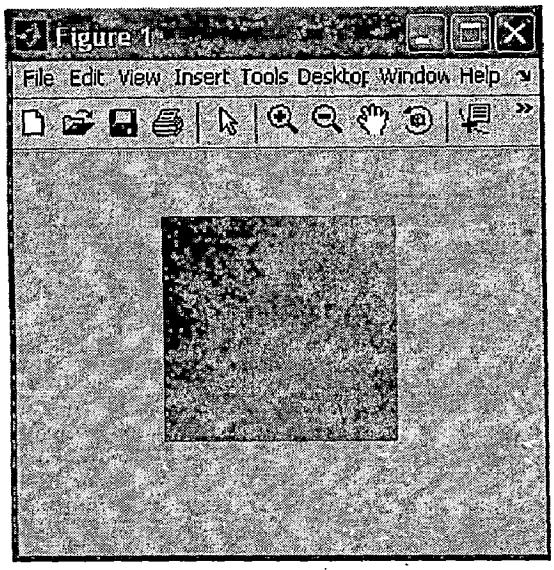

(a) ROI of mammogram "mdb249"

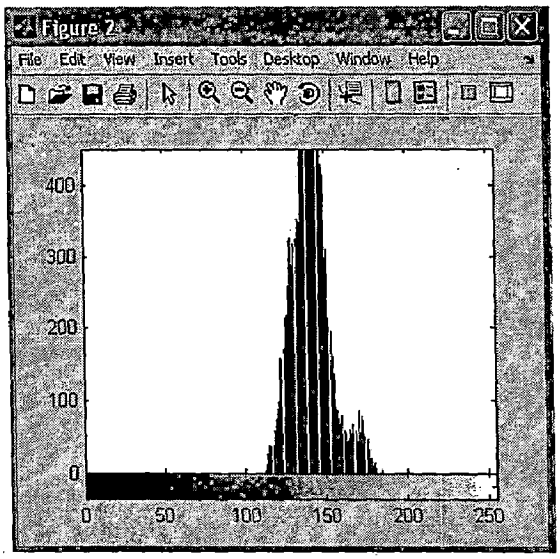

(b) Histogram of (a)

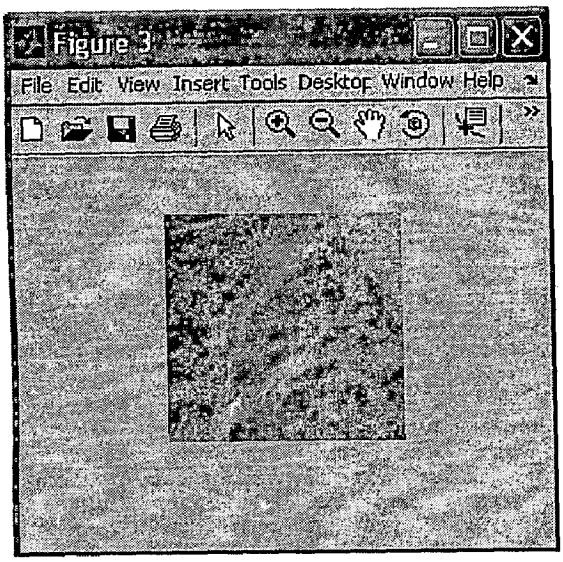

(c) Enhanced image of (a)

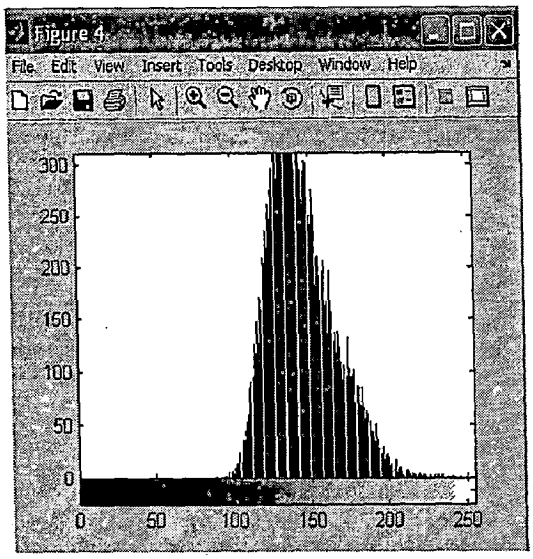

(d) Histogram of (c)

Fig. 3.5 Enhancement by Adaptive Histogram Equalization

3.4. Enhancement by Background removal

The background removal is considered as a necessary procedure in the enhancement of the visibility and detectability of microcalcifications. It is a method of reducing the slowly varying portions of an image, which in turn allows increased gray level variation in image details. It is usually performed by subtracting a low pass-filtered version of the image from itself. Morphological processing methods that have been used successfully for this purpose.

3.4.1. Mathematical Morphological Operations [21]

. The word morphology commonly denotes a branch of biology that deals with the form and structure of animals and plants. We use the same word here in the context of mathematical morphology as a tool for extracting image components that are useful in the representation and description of region shape, such as boundaries, skeletons, and the convex hull. Morphological operations can be employed for many image processing purposes, including edge detection, segmentation, and enhancement of images.

The simplicity of the mathematical morphology comes from the fact that a large class of filters can be represented as the combination of two simple operations on image: the erosion and dilation. Here some fundamental definitions related to morphology are mentioned.

Dilation

The gray-scale dilation of f by structuring element b, denoted $f \oplus b$, is defined as

$$(f \oplus b)(x, y) = \max\{f(x-x', y-y') + b(x', y') \mid (x', y') \in D_b\}$$

Where D_b is the domain of b and f (x, y) is assumed to be equal to $-\infty$ outside the domain of f. This equation implements a process similar to the concept of spatial convolution. Conceptually, we can think of rotating the structuring element about its origin and translating it to all locations in the image, just as the convolution kernel is rotated and then translated about the image. At each translated location, the rotated structuring element values are added to the image pixel values and the maximum is computed.

One important difference between convolution and gray- scale dilation is that, in the latter, D_b, a binary matrix, defines which locations in the neighborhood are included in the max operation. In other words, for an arbitrary pair of coordinates (x_0, y_0) in the domain of D_b, the sum f(x- x_0,y-y_0) + b(x_0,y_0) is included in the max computation only if D_b is 1 at those coordinates. If D_b is 0 at (x_0, y_0), the sum in not considered in the max operation. This is repeated for all coordinates (x', y') $\in D_b$ each time that coordinates (x, y) change. Plotting b(x', y') as a function of coordinates x' and y' would look like a digital "surface" with the height at any pair of coordinates being given by the value of b at those coordinates.

Erosion

The gray-scale erosion of f by structuring element b, denoted $f \Theta b$, is defined as

$$(f \Theta b)(x, y) = \max\{f(x+x', y+y') - b(x', y') \mid (x', y') \in D_b\}$$

Where D_b is the domain of b and f(x, y) is assumed to be $+\infty$ outside the domain of f. conceptually, we again can think of translating the structuring element to all locations in the image. At each translated location, the structuring element values are subtracted from the image pixel values and the minimum is taken.

Opening and Closing

The morphological opening of f by b, denoted $f \circ b$, is simply erosion of f by b followed by dilation of the result by b

$$f \circ b = (f \ominus b) \oplus b$$

this is simply the erosion of f by b, followed by the dilation of the result by b. similarly, the closing of f by b, denoted $f \bullet b$, is dilation followed by erosion.

$$f \bullet b = (f \oplus b) \ominus b$$

both operations have simple geometric interpretations. Suppose that an image function f(x, y) is viewed as a 3-D surface; that is, its intensity values are interpreted as height values over the xy-plane. Then the opening of f by b can be interpreted geometrically as pushing structuring element b up against the underside of the surface and translating it across the entire domain of f. The opening is constructed by finding the highest points reached by any part of the structuring element as it slides against the undersurface of f.

Figure 3.6 is the concept in one dimension. The curve shown 3.6 (a) to be the values along a single row of an image. Figure 3.6(b) shows a flat structuring element in several positions, pushed up against the top of the shaded region in Fig.3.6(c). Since the structuring element is too large to fit inside the upward peak on the middle of the curve, that peak is removed by the opening. In general, openings are used to remove small bright details while leaving the overall gray levels and larger bright features relatively undisturbed.

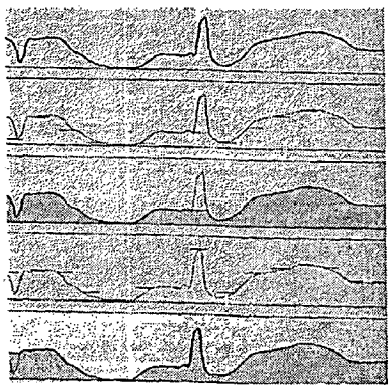

Fig.3.6 (a, b, c, d, e) opening and closing in one dimension

Figure 3. 6(d) provides a graphical illustration of closing. The structuring element is pushed down on top of the curve while being translated to all locations. The closing, shown in fig.3.6 (e), is constructed by finding the lowest points reached by any part of the structuring element as it slides against the upper side of the curve. We can easily see that closing suppresses dark details smaller than the structuring element.

3.4.2 Top-Hat & Bottom-Hat Algorithms

To enhance mammograms using morphological operations, there are two operations, namely, the Top-Hat Transform and the Bottom-Hat Transform.

The Top-Hat Transform is defined as the difference between the original image and its opening. The top-hat transform is used to segment objects that differ in brightness form the surrounding background in the images with uneven background intensity. The top-hat yields an image that contains all the residual features (i.e. peaks and ridges) removed by the opening. Adding these residual features to the original image has the effect of accentuating high-intensity (light) structures.

And the Bottom-Hat Transform defined as the difference between the closing of the original image and the original image. The dual residual (i.e., valleys and troughs) obtained by using the closing is then subtracted from the resulting image to accentuate low-intensity (dark) structures.

If we represent the Top-Hat Transform with TH, Bottom-Hat Transform with BH, and the Original Image with OI, we can extract the high intensity microcalcifications from the mammograms by following operation.

Enhanced Image = OI+TH-BH.

An example is shown below for the morphological enhancement by using top-hat and bottom-hat algorithm for the image "mdb209" in the MIAS Image database.

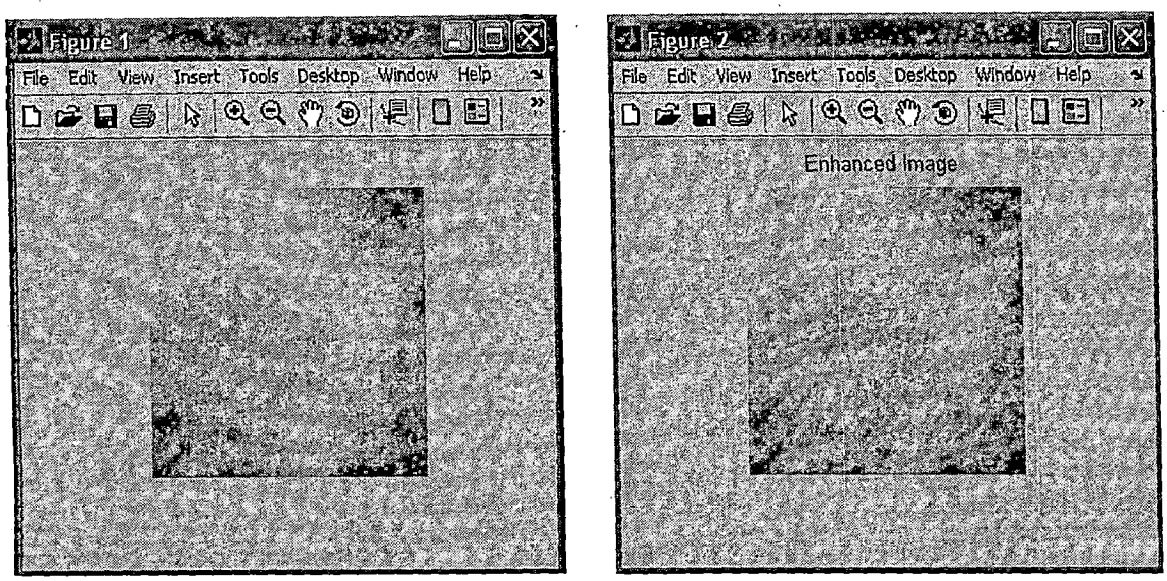

(a) ROI of mdb209 (b) Enhancement of (a)

Fig.3.7 Enhancement by Morphological Methods

AN EVALUATION OF CONTRAST ENHANCEMENT TECHNIQUES OF DIGITAL MAMMOGRAMS

The enhancement results obtained in the previous chapter have been evaluated using various parameters recently proposed in the literature is being discussed in this chapter.

Image enhancement is a necessary component of any CAD system. The principal objective of any enhancement technique is to improve image quality for either an automated CAD framework (e.g., to improve subsequent image segmentation and feature extraction) or for manual reading. Previous work on the enhancement of mammograms has covered a wide range of enhancement techniques. In this context, both standard techniques (Histogram Equalization and Contrast stretching) and novel approaches like Contrast Limited Adaptive Enhancement Techniques, and Morphological Enhancement techniques like top-hat and bottom-hat algorithms have been presented in the previous chapter.

Each of these methods has its own advantages and it has been successfully proved in other application areas that no single image enhancement technique is the dominant solution for all images. Rule-based systems and machine learning techniques are increasingly being explored to predict the best-suited image enhancement algorithm for a given test image out of several available [23-24]. Such machine learning approaches are heavily dependent on the quantitative estimates of what is automatically judged to be a good image enhancement. It is, therefore, important to define quantitative measures for defining the quality of image enhancement that correlates well with the human expert but does not require human intervention for making such a judgment [22].

The problem of objective measurement of image enhancement quality can be defined as follows. Given an image, and a set of image enhancement techniques (e1,e2,e3,...eM) , whose application produces output images (I1,I2,I3,...IM), the aim is to mathematically define a set of metrics (m1,m2,m3,...mN), each of which is bounded within a [0,1] range, that measure the quality of image enhancement. The measurement range represents a continuous spectrum of values that each metric can take, with 0 defining the worst possible image enhancement and 1 representing the

best possible enhancement. Ideally, a simple scheme should also exist which either linearly or nonlinearly combines N the metrics (m1,m2,m3,... mN) into a single composite measure that is bounded between [0,1] range and defines the quality of image enhancement.

In the context of digital mammography, the ability of an enhancement technique to improve the contrast between the target region(s) of interest (ROI), which represents a possible area of microcalcifications, and its background is extremely important. This concept defines the nature of the metrics. In the next section, three metrics have been proposed that objectively measure the degree of contrast between the target and background pixels.

4.1 Mammographic Enhancement Methods

In order to evaluate the significance of our quantitative metrics of image enhancement on a number of test images, a total of four enhancement techniques have been used. The first method is fairly established, Histogram Equalization, which has been frequently, used as a simple image enhancement method in a number of studies. The second method is also an established one, namely Contrast stretching.

In addition to the two above mentioned methods, recently developed Contrast Limited Adaptive Histogram Equalization and Morphological Enhancement methods have been used. These methods and their corresponding results have been discussed in the previous chapter. The aim is to apply each of these techniques for each image tested, and then evaluate their performance on the basis of newly developed quantitative measurements of mammographic contrast enhancement as discussed in the next section.

4.2 Quantitative Measures of Mammographic Contrast Enhancement

This section introduces and describes the quantitative measures of enhancement used in this study. Each method is described and in turn concluded with a novel method of combining them, thereby giving a single measure of enhancement performance. The aim of these measures is to quantify the degree of contrast between

the target (ROI of microcalcifications) and the background (area surrounding the microcalcifications), as shown in fig.4.1

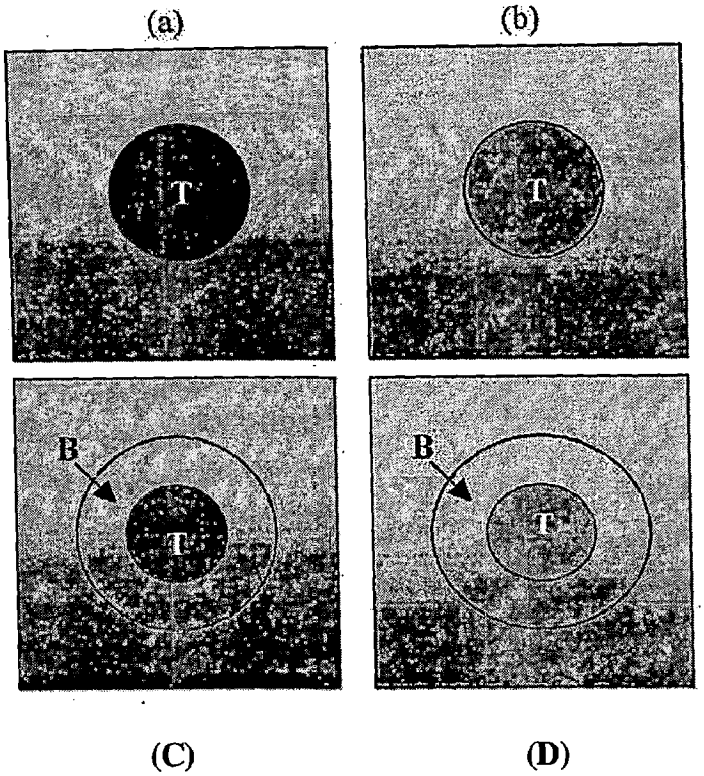

Fig.4.1 Target T and background B [original image (a) is enhanced as (b), analysis images are (c) and (d)] ref:[22]

In this figure, the original image (a) that is enhanced to produce image (b). For our analysis we do not need to know the details of the enhancement process. The boundary of the ROI has been delineated and labels it as the target T. Because of the potentially large variations of intensities outside of the ROI and across the rest of the image, a boundary has been constructed to the background B. This reflects the subconscious act of human perception in viewing a target against a locally enclosed neighborhood background. The background B here is shown as the region outside the target marked by a concentric circle. The boundaries for Fig. 2.1(a) and (b) are shown in Fig.2.1(c) and (d). By extracting the grayscale intensities from these two regions, we are able to calculate quantitative measures for analyzing the improvement in image quality as a result of the enhancement process.

4.2(a) Distribution Separation Measure (DSM)[22]

Using the method for labeling the target (T) an background (B) regions described, we can plot the overlap of the density functions for the grayscales comprising these two regions as shown in Fig. 4.2

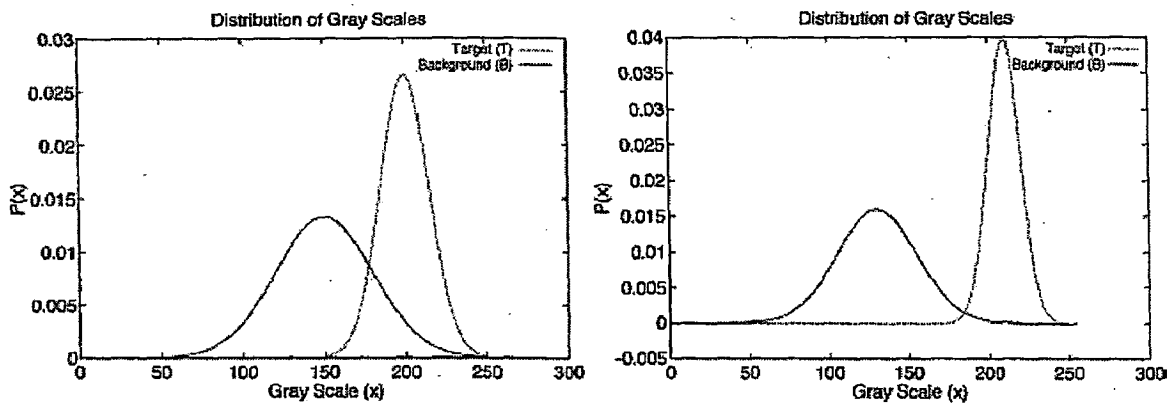

Fig.4.2 Distribution overlap between background and target before and after enhancement

In mammography, this is representative of the overlap found between ROI of microcalcifications and the background boarder. A good enhancement technique should ideally reduce the overlap. In particular, we expect that the enhancement technique should help reduce the spread of the target distribution and shift its mean grayscale level to a higher value, thus separating the two distributions and reducing their overlap. The best decision boundary for the original image between the two classes is a weighted average of the group centroids will provide an optimal cutting score.

$$D_1 = \mu_B^O N_T^O + \mu_T^O N_B^O /(N_B^O + N_T^O) \qquad \text{----(4.1)}$$

And

$$D_2 = \mu_B^E N_T^E + \mu_T^E N_B^E /(N_B^E + N_T^E) \qquad \text{----(4.2)}$$

Where N_B^O and N_T^O are the number of samples in the background and target prior to enhancement, and N_B^E and N_T^E are the respective sample number after the enhancement. Again this approximation assumes that the two distributions are normal and that the group dispersion structures are known. By combining (4.1) and (4.2), we

can compute a distance measure between the decision boundaries and the mean of the targets and background, before and after segmentation. This is termed as DSM, and proposes it is a measure of quality of enhancement. This is defined as

$$DSM = (\mid \mu_T^E - \mu_B^E \mid) - (\mid \mu_T^O - \mu_B^O \mid) \qquad \text{----(4.3)}$$

Ideally, the measurement should be greater than zero: the greater the DSM value, the better the quality of enhancement. For comparing any two enhancement techniques, we should choose the technique that gives a higher value on DSM measure.

4.2(b) Target-to-Background Contrast Enhancement Measurement Based on Standard Deviation (TBC_S)

A key objective of a contrast enhancement is to maximize the difference between background and target mean gray level and ensure that the homogeneity of the mass is increased aiding the visualization of its boundaries and location. Using the ratio of

the standard deviation n of the grayscales within the target before and after the enhancement, we can quantify this improvement using the TBC_S given in Eq. (4.4)

$$TBC_S = ((\mu_T^E / \mu_B^E) - (\mu_T^O / \mu_B^O))/(\sigma_T^E / \sigma_T^O) \qquad \text{----(4.4)}$$

It is expected that as a result of enhancement, this measure should give a value greater than zero.

4.2(c) Target-to-Background Contrast Enhancement Measurement Based on Entropy (TBC_E)

The concept of TBC_S can be extended further by replacing the standard deviation with the entropy of the target in the original and enhanced images, ε_T^E and ε_T^O, respectively, to quantify the homogeneity ratio. The TBC_E is defined as

$$TBC_E = ((\mu_T^E / \mu_B^E) - (\mu_T^O / \mu_B^O))/(\varepsilon_T^E / \varepsilon_T^O) \qquad \text{----(4.5)}$$

It is expected that as a result of enhancement, this measure should give a value greater than zero. Entropy is a statistical measure of randomness that can be used to characterize the texture of the input image.

Entropy is defined as

e = -sum(p.*log(p))

where p contains the histogram counts

4.3 Combined Enhancement Measure (D)

Although the measures described above have proved to correlate well previously [22], there is a need of a method to combine the measures into one quantitative value. Using this combined measure, we will be able to quantitatively rank enhancement techniques for a particular image. To combine DSM, TBC_E, and TBC_S for a particular enhancement, we represent each enhancement value within a three-dimensional Euclidean space by scaling each within the range [0, 1]. Each of the measure has been given the same weight and a simple min-max scaling has been applied. A high-performance contrast enhancement method will have points close to coordinates (1, 1, 1). We compute the combined measure D by calculating the Euclidean distance between the point in the 3-D coordinate space representing the enhancement and (1,1,1), the best possible enhancement using

$$D = sqrt((1-DSM)^2 + (1-TBC_S)^2 + (1-TBC_E)^2) \qquad \text{----(4.6)}$$

The enhancement method giving the smallest value of D is selected as the best enhancement method for this image.

From target and background regions identified in the original and enhanced images, we extract each measure and use them to formulate the combined measure D.

4.3 Mammographic Database

The use of international mammographic databases is important as this allows comparison of results from different studies. The Mammographic Image Analysis Society (MIAS) Mini Mammographic Database [8], which contains 322 mammograms including normal, mass, and microcalcification cases, have been used. The image size in the Mini Mammographic database has been clipped and padded to become 1024×1024 pixels whose spatial resolution is 200μm and dynamic range is 8-bit. In this work, the microcalcifications of 0.05 to 1.0 mm in diameter are of interest, which corresponding to one to five pixels in diameter. The Image Database is provided with the character of background tissues like Fatty, Dense-Glandular etc., class of abnormality presented i.e., calcifications, speculated masses etc., severity of abnormality i.e., malignant or benign, center coordinates of abnormality and radius of

the abnormality. This information will help in finding the Region of Interest (ROI), and its background.

Here some of the enhancement techniques and their qualitative and quantitative measures have been provided. As discussed earlier, four enhancement techniques have been compared using the DSM, TBC_S, TBC_E and D. A final conclusion has been drawn on each mammogram based on the value of D. The minimum the value of D, the greater the enhancement method.

From the MIAS database, five mammographic images have been studied, which are malignant cases. The images are mdb209, mdb213, mdb233, mdb241, mdb249.

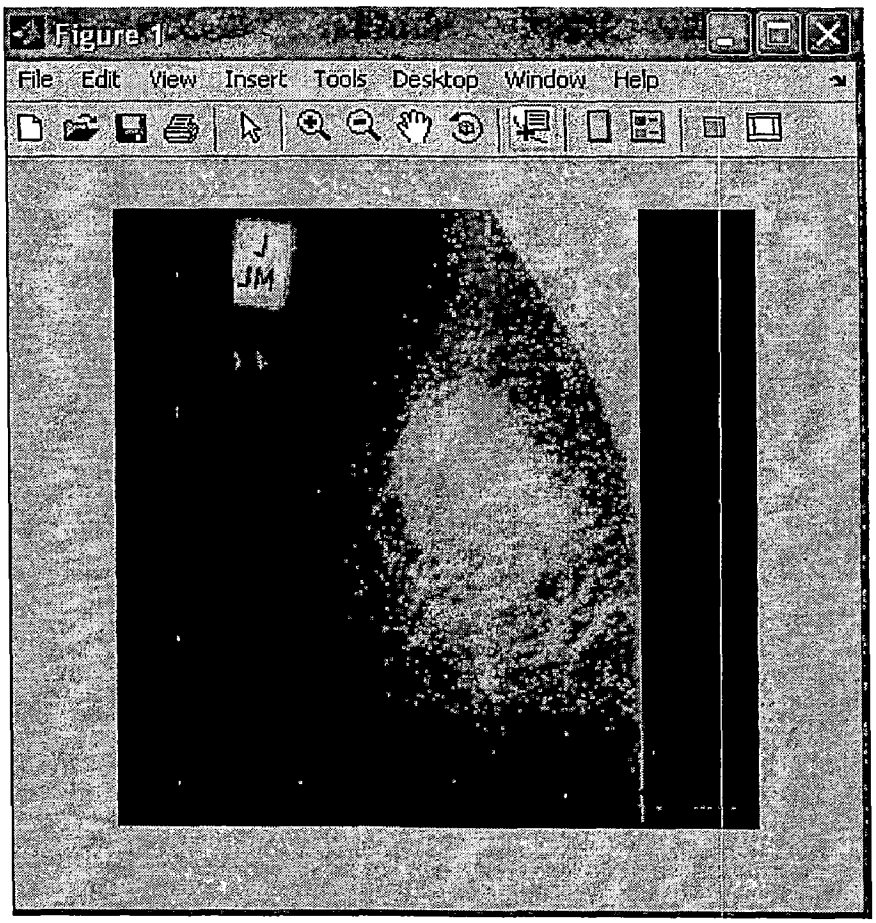

Fig.4.3 Mammogram mdb209

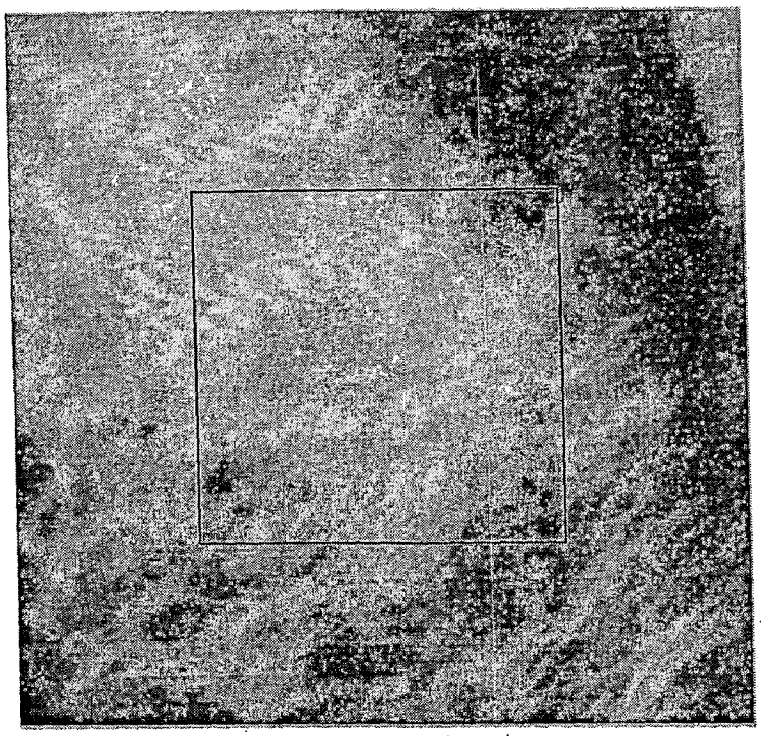

Fig.4.4 ROI and its Background of mdb209 [8]

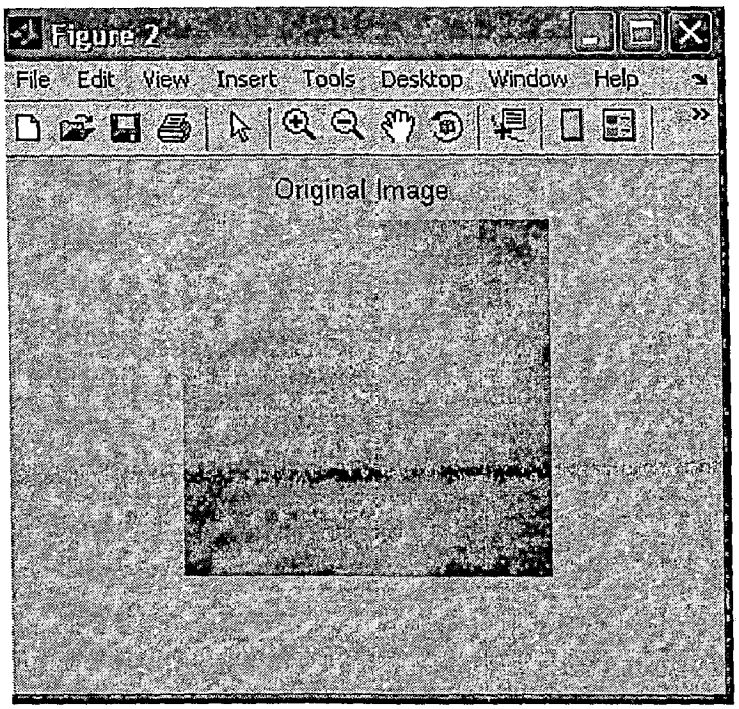

Fig.4.5 ROI of mdb209

Here, the computational values of DSM, , TBC_S, TBC_E and D for various images have been tabled.

Mdb209

METHOD	DSM	TBCs	TBCe	D
HISTOGRAM EQUALIZATION	0.1759	0.2251	0.5603	1.2137
ADAPTIVE HISTOGRAM EQ.	0.1800	0.2400	0.5879	1.1903
CONTAST ENHANCEMENT	0.1600	0.2350	0.5929	1.2069
MORPHOLOGICAL OPERATIONS	0.0925	0.2420	0.5879	1.3333

Mdb213

METHOD	DSM	TBCs	TBCe	D
HISTOGRAM EQUALIZATION	0.1821	0.1175	0.4739	1.3132
ADAPTIVE HISTOGRAM EQ.	0.0932	0.0673	0.2134	1.5202
CONTRAST ENHANCEMENT	0.1456	0.1049	0.3523	1.3967
MORPHOLOGICAL OPERATIONS	0.0425	0.0385	0.1984	1.5760

Mdb233

METHOD	DSM	TBCs	TBCe	D
HISTOGRAM EQUALIZATION	0.0532	0.0019	0.0110	1.6943
ADAPTIVE HISTOGRAM EQ.	0.1030	0.0044	0.0201	1.6601
CONTRAST ENHANCEMENT	0.0743	0.0020	0.0154	1.6800
MORPHOLOGICAL OPERATIONS	0.0987	0.0043	0.0190	1.6632

Mdb241

METHOD	DSM	TBCs	TBCe	D
HISTOGRAM EQUALIZATION	0.0143	0.0029	0.0047	1.7194
ADAPTIVE HISTOGRAM EQ.	0.0382	0.0668	0.0662	1.6334
CONTRAST ENHANCEMENT	0.0286	0.0063	0.0099	1.7063
MORPHOLOGICAL OPERATIONS	0.0192	0.0050	0.0080	1.7135

Mdb249

METHOD	DSM	TBCs	TBCe	D
HISTOGRAM EQUALIZATION	0.1099	0.0593	0.2608	1.4912
ADAPTIVE HISTOGRAM EQ.	0.0009	0.0112	0.0325	1.7065
CONTRAST ENHANCEMENT	0.0263	0.0261	0.0593	1.6678
MORPHOLOGICAL OPERATIONS	0.0011	0.0014	0.0017	1.7296

So from the above tables, we can find that there is no unique enhancement technique is sufficient for all images. Each image gives different optimum enhancement technique.

Transformation Methods for Microcalcification Detection

Wavelets are mathematical functions that decompose the input data into different frequency components, and then study each component with a resolution matched to its scale. They have advantages over traditional Fourier methods in analyzing physical situations where the signal contains discontinuities and sharp spikes. Wavelets were developed independently in the fields of mathematics, quantum physics, electrical engineering, and seismic geology. Interchanges between these fields during the last ten years have led to many new wavelet applications such a s biomedical applications, turbulence, human vision, radar, and earthquake prediction. For better understanding and appreciation of the need for developing the wavelet transform, the chronology of developments needs to be revisited, which greatly influenced the idea of coming up with the new transform.

Chronology of developments [16, 17]

Mathematical transformations are applied to signals to obtain further information from that signal that is not readily available in the raw signal. There are number of transformations that can be applied, among which the Fourier Transform are probably by far the most popular.

Most of the signals in practice are **time-domain** signals in their raw format. That is, whatever that signal is measuring, is a function of time. In other words, when we plot the signal one of the axis is time (independent variable), and the other (dependent variable) is usually the amplitude. When we plot time-domain signals, we obtain a **time-amplitude representation** of the signal. This representation is not always the best representation of the signal for most signal processing related applications. In many cases, the most distinguished information is hidden in the frequency content of the signal. The **frequency spectrum** of a signal is basically the frequency components (spectral components) of that signal. The frequency spectrum of a signal shows what frequencies exist in the signal.

Intuitively, we all know that the frequency is something to do with the change in rate of something. If something (a mathematical or physical variable would be the technically correct term) changes rapidly, we say that it is of high frequency, where as if this variable does not change rapidly, i.e., it changes smoothly, we say that it is of low frequency. If this variable does not change at all, then we say it has zero frequency, or no frequency. For example the publication frequency of a daily newspaper is higher than that of a monthly magazine (it is published more frequently).

5.1 Fourier Analysis

Although FT is probably the most popular transform being used (especially in electrical engineering), it is not the only one. There are many other transforms that are used quite often by engineers and mathematicians. Hilbert transform, short-time Fourier transform (more about this later), Wigner distributions, the Radon Transform, and of course our featured transformation , the wavelet transform, constitute only a small portion of a huge list of transforms that are available at engineer's and mathematician's disposal. Every transformation technique has its own area of application, with advantages and disadvantages, and the wavelet transform (WT) is no exception.

For a better understanding of the need for the WT we need to look at the FT more closely. FT (as well as WT) is a reversible transform, that is, it allows to go back and forward between the raw and processed (transformed) signals. However, only either of them is available at any given time. That is, no frequency information is available in the time-domain signal, and no time information is available in the Fourier transformed signal. The natural question that comes to mind is that is it necessary to have both the time and the frequency information at the same time?

As it can be seen subsequently, the answer depends on the particular application and the nature of the signal in hand. Recall that the FT gives the frequency information of the signal, which means that it tells us how much of each frequency exists in the signal, but it does not tell us when in time these frequency components exist. This information is not required when the signal is so-called stationary

It is required to take closer look at this stationarity concept more closely, since it is of paramount importance in signal analysis. Signals whose frequency content do not change in time are called stationary signals. In other words, the frequency content of stationary signals do not change in time. In this case, one does not need to know at what times frequency components exist, since all frequency components exist at all times.

For example the following signal

x(t)=cos(2*pi*10*t)+cos(2*pi*25*t)+cos(2*pi*50*t)+cos(2*pi*100*t)

is a stationary signal, because it has frequencies of 10, 25, 50, and 100 Hz at any given time instant. The signal can be plotted as shown in the below figure:

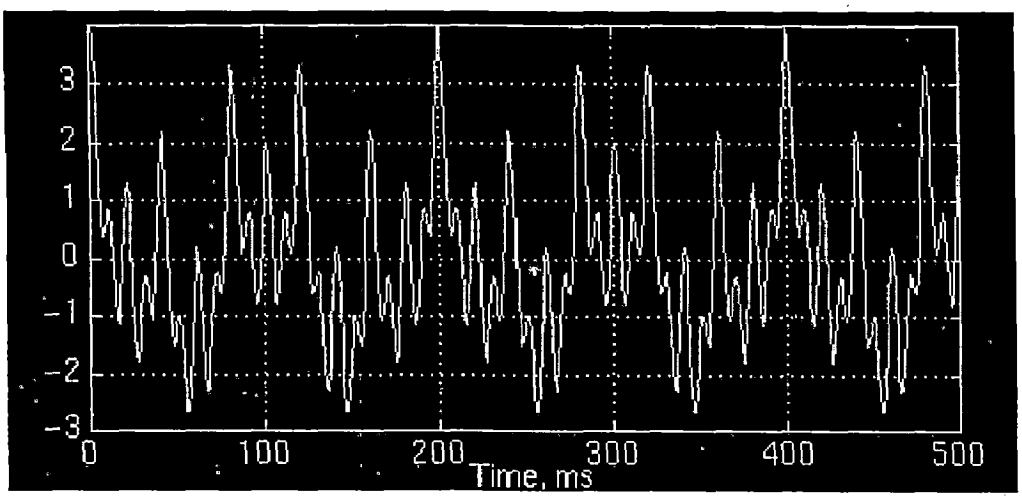

Fig 5.1 Plot of x(t)

And the following is its FT:

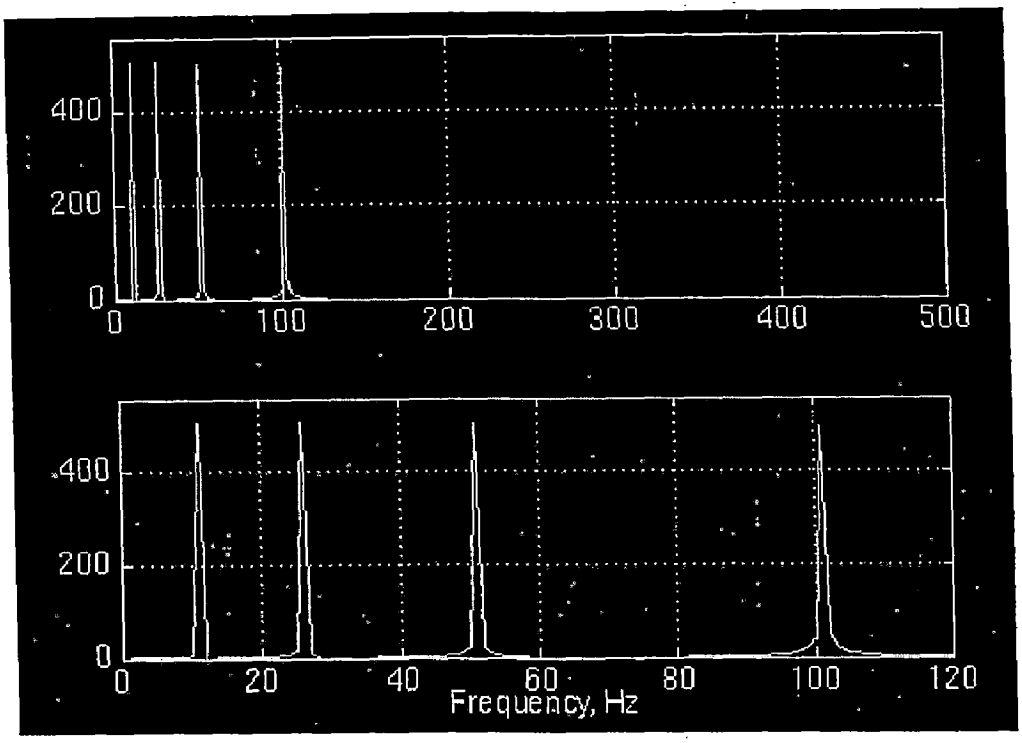

Fig 5.2 Fourier transform of x(t)

The top plot in figure 5.2 is the (half of the symmetric) frequency spectrum of the signal in figure 5.1. The bottom plot is the zoomed version of the top plot, showing only the range of frequencies that are of interest to us. Note the four spectral components corresponding to the frequencies 10, 25, 50 and 100.

Contrary to the signal in Figure 5.1, the following signal is not stationary. Figure 5.3 plots a signal whose frequency constantly changes in time. This signal is known as the "chirp" signal. This is a non-stationary signal.

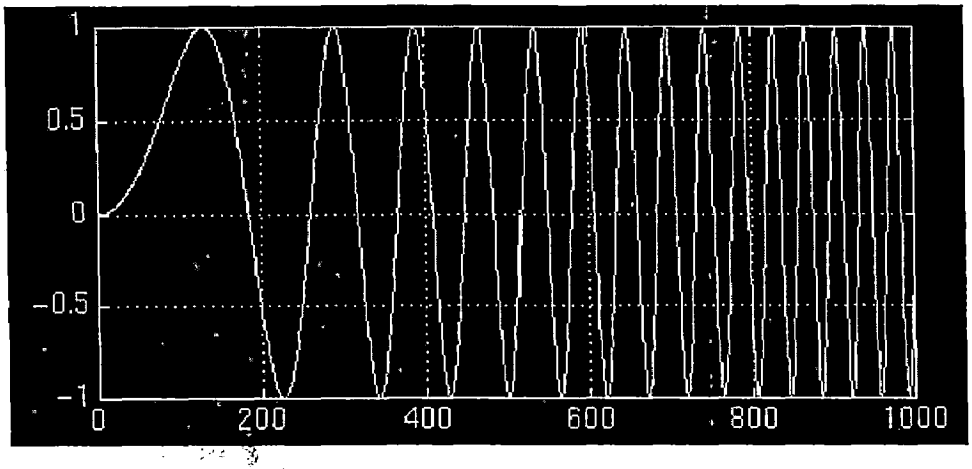

Fig 5.3 Non-stationary signal

The Figure 5.4(a) plots a signal with four different frequency components at four different time intervals, hence a non-stationary signal. The interval 0 to 300 ms has a 100 Hz sinusoid, the interval 300 to 600 ms has a 50 Hz sinusoid, the interval 600 to 800 ms has a 25 Hz sinusoid, and finally the interval 800 to 1000 ms has a 10 Hz sinusoid.

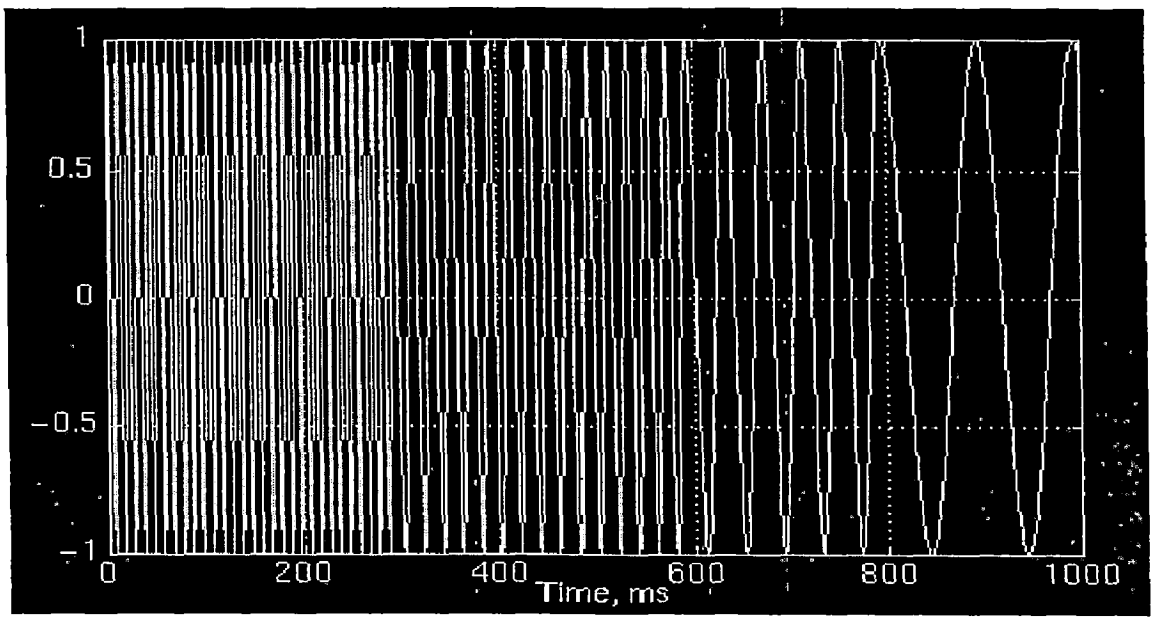

Fig 5.4 Non-stationary signal with different frequency components

And the following is its FT

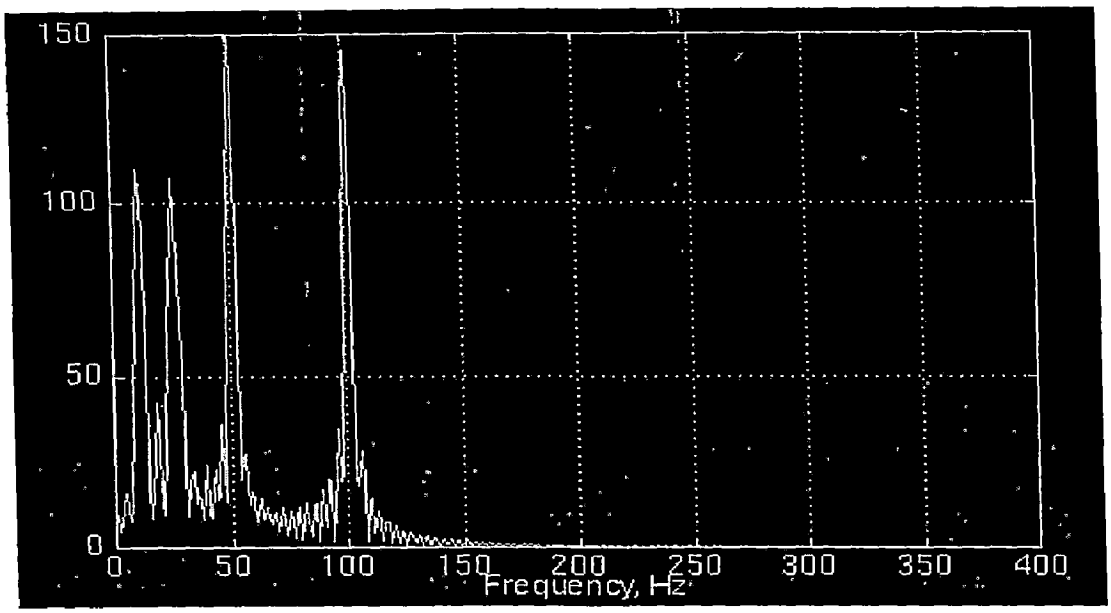

Fig 5.5 FT of non-stationary signal.

The little ripples at this time; they are due to sudden changes from one frequency component to another, which have no significance in this text. Note that the amplitudes of higher frequency components are higher than those of the lower frequency ones. This is due to fact that higher frequencies last longer (300 ms each) than the lower frequency components (200 ms each). Other than those ripples, everything seems to be right. The FT has four peaks, corresponding to four frequencies with reasonable amplitude.

For the first signal, plotted in figure 5.1, consider the following question i.e., "At what times (or time intervals), do these frequency components occur?" and the answer would be : At all times. Therefore, in stationary signals, all frequency components that exist in the signal exist throughout the entire duration of the signal. There is 10 Hz at all times, there is 50 Hz at all times, and there is 100 Hz at all times. Now, consider the same question for the non-stationary signal in figure 5.3 or in figure 5.4, "At what times these frequency components occur?" For the signal in figure 5.4, we know that in the first interval we have the lowers frequency component. For the signal in figure 5.3, the frequency components change continuously. Therefore, for these signals the frequency components do not appear at all times.

Now, compare the Figures 5.2 and 5.5. The similarity between these two spectrum should be apparent. Both of them show four spectral components at exactly the same frequencies, i.e., at 10, 25, 50, and 100 Hz. Other than the ripples, and the difference in amplitude (which can always be normalized), the two spectrums are almost identical, although the corresponding time-domain signals are not even close to each other. Both of the signals involves the same frequency components, but the first one has these frequencies at all times, the second one has these frequencies at different intervals. So, how come the spectrums of two entirely different signals look very much alike? Recall that the FT gives the spectral content of the signal, but it gives no information regarding where in time those spectral components appear.

Therefore, FT is not a suitable technique for non-stationary signal, with one exception: FT can be used for non-stationary signals, if we are only interested in what spectral components exist in the signal, but not interested where these occur. However, if this information is needed, i.e., if we want to know, what spectral component occur at what time (interval) , then Fourier transform is not the right transform to use.

For practical purposes it is difficult to make the separation, since there are a lot of practical stationary signals, as well as non-stationary ones. Almost all biological signals, for example, are non-stationary. Some of the most famous ones are ECG (electrical activity of the heart, electrocardiograph), EEG (electrical activity of the brain, electroencephalograph), and EMG (electrical activity of the muscles, electromyogram).

"Therefore it can be inferred that, the FT gives what frequency components (spectral components) exist in the signal. Nothing more, nothing less".

When the time localization of the spectral components is needed, a transform giving the time-frequency representation of the signal is needed.

5.2 Short time Fourier Analysis [3, 12]:

In an effort to correct this deficiency, Dennis Gabor adapted the Fourier transform to analyze only a small section of the signal at a time i.e., a technique called *windowing* the signal. Gabor's adaptation called Short-time Fourier Transform (STFT), maps a signal into a two-dimensional function of time and frequency, the same is depicted in figure 5.6

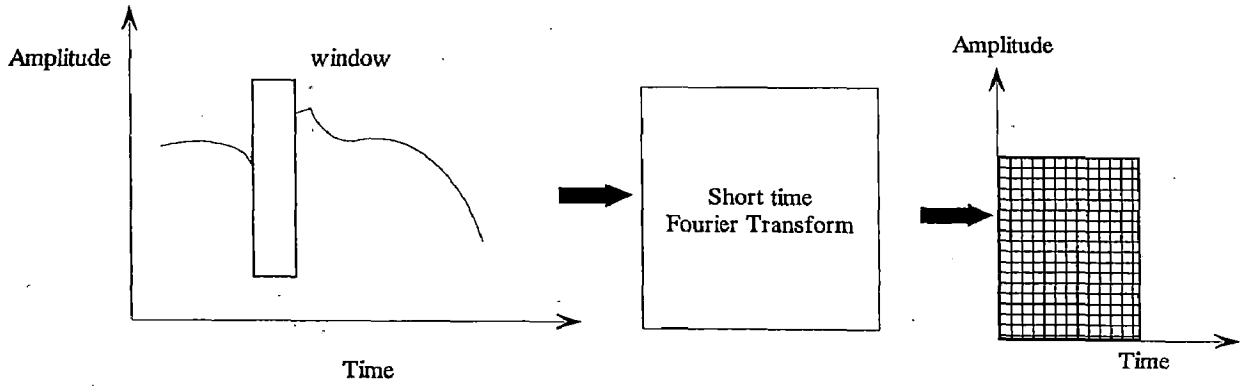

Fig 5.6 STFT Process

The STFT represents a sort of compromise between the time and frequency based views of a signal. It provides some information about both when and at what frequencies a signal event occurs. However, we can only obtain this information with limited precision, and that precision is determined by the size of the window.

While the STFT compromise between time and frequency information can be useful, the drawback is that once you choose a particular size for the time window, that window is the same for all frequencies. Many signals require a more flexible approach: one where we can vary the window size to determine more accurately either time or frequency, to understand why researches switched over to the development of WT from the existing STFT, prior knowledge of uncertainty principle and problem of resolution is a must.

The uncertainty principle, originally found and formulated by Heisenberg, states that "the momentum and the position of a moving particle cannot be known simultaneously." This applies to our above argument as follows:

The frequency and time information of a signal at some certain point in the time-frequency plane cannot be known. In other words, "we cannot know what spectral component exists at any given time instant. The best we can do is to investigate what spectral components exist at any given interval of time". This is a problem of resolution [17], and it is the main reason why researchers had switched over to WT from STFT.

STFT gives a fixed resolution at all times, whereas WT gives a variable resolution as follows:

Higher frequencies are better resolved in time, and lower frequencies are better resolved in frequency. This means that, a certain high frequency component can be located better in time (with less relative error) than a low frequency component. The wavelet analysis in the next section would better explain the problem of resolution.

5.3 Wavelet Analysis [3, 12]:

Wavelet analysis represents the next logical step: a windowing technique with variable-sized regions. Wavelet analysis allows the use of long time intervals where we want more precise low-frequency information, and shorter regions where we want high frequency information (figure 5.7).

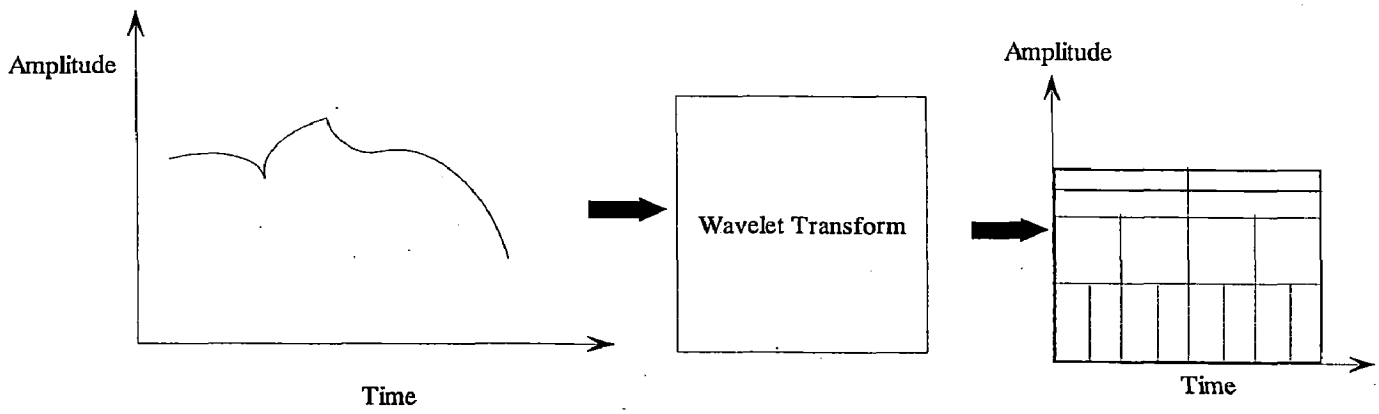

Fig.5.7 Wavelet Analysis

Here's (as given in fig 5.8) what this looks like in contrast with the time-based, frequency-based, and STFT views of a signal.

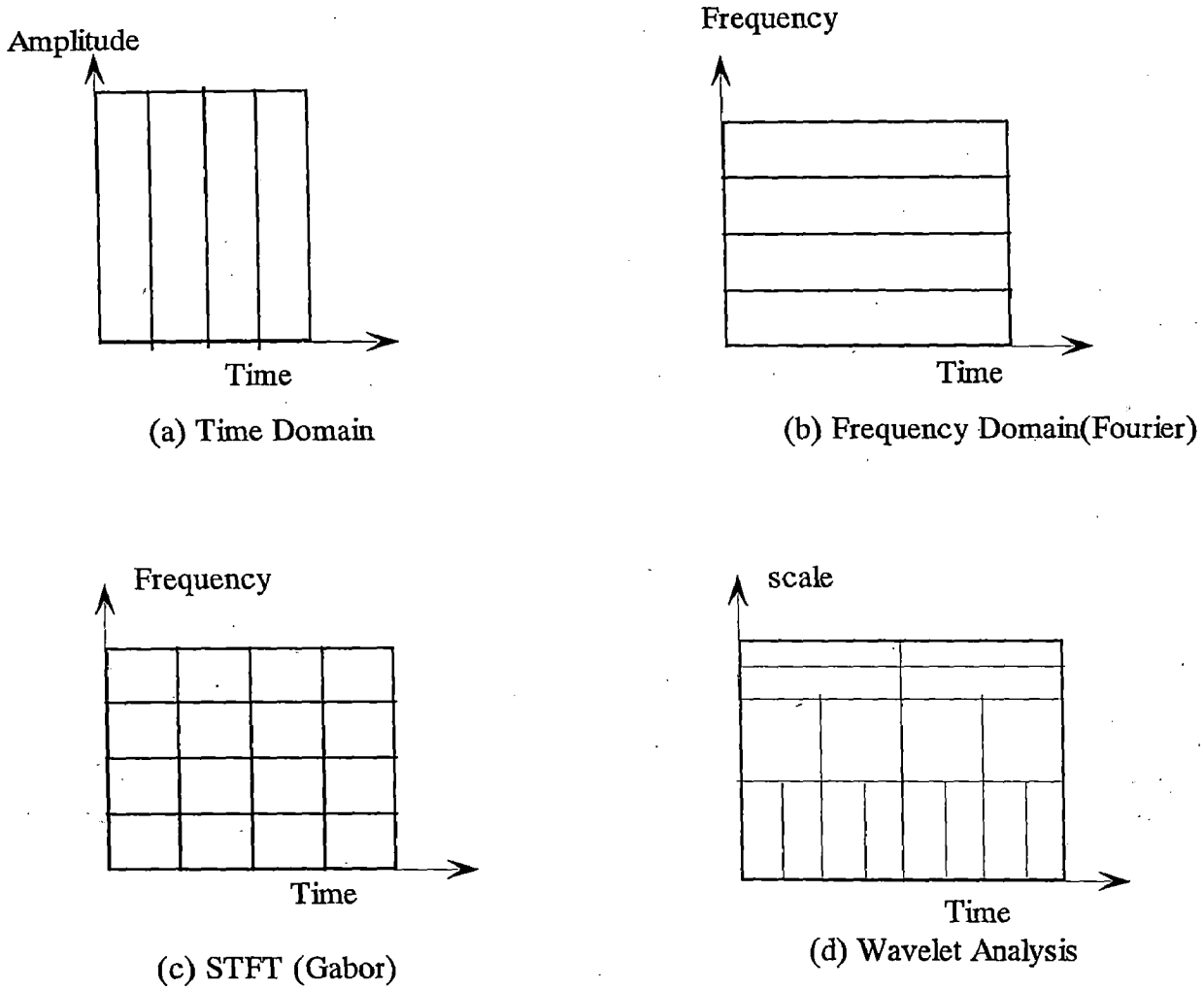

Fig 5.8 comparison between domains

So we can conclude that wavelet analysis allows to get the information in the frequency domain and at the same time allows to view the image or function at different resolutions.

As the microcalcifications are not clearly visible directly in the original resolution of the mammograms, we have to decompose the image into different resolutions. This is achieved only with the help of the wavelet analysis. The detection of the microcalcifications is explained in the next chapter.

MULTIRESOLUTION ANALYSIS AND DETECTION OF MICROCALCIFICATIONS

Although the Fourier transform has been the mainstay of transform-based image processing since the late 1950s, a more recent transformation, called the wavelet transform, is now making it even easer to analyze, compress and transmit many images. Unlike the Fourier transform, whose basis functions are sinusoids, wavelet transforms are based on small waves, called *wavelets*, of varying frequency and *limited duration*. This allows them to provide the equivalent of a musical score for an image, revealing not only what notes (or frequencies) to play but also when to play them [24].

In 1987, wavelets were first shown to be the foundation of a powerful new approach to signal processing and analysis called *multiresloution* theory. (Mallet [1987]). Multiresolution theory incorporates and unifies techniques from a variety of disciplines, including subband coding from signal processing, quadrature mirror filtering from digital speech recognition, and pyramidal image processing. As its name implies, Multiresolution theory is concerned with their representation and analysis of images at more than one resolution. The appeal of such an approach is obvious – features that might go undetected at one resolution may be easy to spot at another.

6.1 Multiresolution Expansions

When we look at images, generally we see connected regions of similar texture and gray level that combine to form objects. If the objects are small in size or low in contrast, we normally examine them at high resolutions: if they are large in size or high in contrast, a coarse view is all that is required. If both small and large objects – or low and high contrast objects – are present simultaneously, it can be advantageous to study them at several resolutions. This, of course, is the fundamental motivation for multiresloution processing.

Image Pyramids, Subband coding and Haar Transform played an important role in the development of a unique mathematical theory called multiresloution analysis (MRA). In MRA, a *scaling function* is used to create a series of approximations of a function or image, each differing by a factor of 2 from its nearest neighboring approximations. Additional functions, called *wavelets*, are then used to encode the difference in information between adjacent approximations.

6.1.1 Series Expansions

A signal or function f(x) can often be better analyzed as a linear combination of expansion functions

$$f(x) = \sum_k \alpha_k . \, _k(x) \qquad \text{---- (6.1)}$$

Where k is an integer index of the finite or infinite sum, the α_k (x) are real-valued expansion coefficients, and the $\phi_{k(x)}$ are real-valued expansion functions. If the expansion is unique – that is, there is only one set of α_k for any given f(x) – the $\phi_{k(x)}$ are called *basis functions*, and the *expansion set,* $\{\phi_{k(x)}\}$, is called a *basis* for the class of functions that can be so expressed. The expressible functions form a *function space* that is referred to as the *closed span* of the expansion set, denoted

$$V = \overline{span\{\phi_{k(x)}\}} \qquad \text{---- (6.2)}$$

To say that f(x)∈ V means that f(x) is in the closed span of $\{\phi_{k(x)}\}$ and can be written in the form of Eq. 6.1

For any function space V and corresponding expansion set$\{\phi_{k(x)}\}$, there is a set of *dual* functions, denoted $\{\tilde{\phi}_k(x)\}$, that can be used to compute the α_k coefficients of Eq.6.1 for any f(x)∈V. these coefficients are computed by taking the *integral inner products* of the dual $\tilde{\phi}_k(x)$'s and function f(x), that is,

$$\alpha_k = <\tilde{\phi}_k(x), f(x)> = \int \tilde{\phi}_k^{*}(x) f(x) dx \qquad \text{----(6.3)}$$

Where the * denotes the complex conjugate operation. Depending on the orthogonality of the expansion set, this computation assumes one of three possible forms as mentioned below.

Case 1: If the expansion functions form an orthonormal basis for V, meaning that

$$< \phi_j(x), \phi k(x) >= \phi_{jk} = \begin{cases} 0 & j \neq k \\ 1 & j = k \end{cases} \qquad \text{---- (6.4)}$$

The basis and its dual are equivalent. That is, $\phi_{k(x)} = \phi_k^*(x)$ and Eq. 6.3 becomes

$$\alpha k = <\phi k(x), f(x)> \qquad \text{----- (6.5)}$$

The α_k are computed as the inner products of the basis functions and f(x).

Case 2: If the expansion functions are not orthonormal, but are an orthogonal basis, for V, then

$$< \varphi j(x) \varphi k(x) >= 0 \quad j \neq k) \qquad \text{---- (6.6)}$$

And the basis functions and their duals are called biorthogonal. The α_k are computed using Eq.(6.6), and biorthogonal basis and its dual are such that

$$< \phi_j(x), \tilde{\phi} k(x) >= \phi_{jk} = \begin{matrix} 0 & j \neq k \\ 1 & j = k \end{matrix} \qquad \text{---- (6.7)}$$

Case 3: If the expansion set is not a basis for V, but supports the expansion defined in Eq.(6.1), it is a spanning set in which there is more than one set of α_k for any $f(x) \in V$. The expansion functions and their duals are said to be overcomplete or redundant. They form a frame in which

$$A\|f(x)\|^2 \leq \sum_k |< \phi_k(x), f(x) >|^2 \leq B\|f(x)\|^2 .$$

For some $A > 0, B < \infty$, and all $f(x) \in V$. Dividing this equation by the norm squared of f(x), we see that A and B "frame" the normalized inner products of the expansion coefficients and the function. If A=B, the expansion set is called a tight frame and it can be shown that

$$f(x) = 1/A \sum_k < \phi_k(x), f(x) > \phi_k(x)$$

Except for the A^{-1} term, which is a measure of the frame's redundancy, this is identical to the expression obtained by substituting Eq (6.5) into Eq (6.1)

6.1.2 Scaling Functions

Now consider the set of expansion functions composed of integer translations and binary scalings of the real, square – integrable function $\phi(x)$; that is, the set $\{\phi_{j,k}(x)\}$, where

$$\phi_{j,k}(x) = 2^{j/2}\phi(2^j x - k) \qquad \text{---- (6.8)}$$

For all j, k$\in$Z and $\phi(x) \in L^2(R)$. Here, k determines the position of $\phi_{j,k}(x)$ along the x-axis, j determines $\phi_{j,k}(x)$'s width – how broad or narrow it is along the x-axis – and $2^{j/2}$ controls its height or amplitude. Because the shape of $\phi_{j,k}(x)$ changes with j, $\phi(x)$ is called a *scaling function*. By choosing $\phi(x)$ wisely, $\{\phi_{j,k}(x)\}$ can be made to span $L^2(R)$, the set of all measurable, square – integrable functions.

If we restrict j in Eq. (6.8) to a specific value, say j= j_0, the resulting expansion set, $\{\phi_{j0,k}(x)\}$, is a subset of $\{\phi_{j,k}(x)\}$. It will not span $L^2(R)$, but a subspace within it. Using the notation of the previous section, we can define that subspace as

$$V_{j0} = \overline{span}_k\{\phi_{j0,k}(x)\} \qquad \text{---- (6.9)}$$

That is, V_{j0} is the span of $\phi_{j0,k}(x)$ over k. If f(x)$\in$ V_{j0}, it can be written

$$f(x) = \sum_k \alpha_k \phi_{j0,k}(x) \qquad \text{---- (6.10)}$$

More generally, we will denote the subspace spanned over k for any j as

$$V_j = \overline{span}_k\{\phi_{j,k}(x)\} \qquad \text{---- (6.11)}$$

When we increase the size of j, it causes the increase of V_j, allowing functions with smaller variations or finer detail to be included in the subspace. This is a consequence of the fact that, as j increases, the $\phi_{j,k}(x)$ that are used to represent the subspace functions become narrower and separated by smaller changes in x.

The scaling function has to obey four fundamental requirements of multiresloution analysis ([Mallet [1989]]).

MRA Requirement 1: The scaling function is orthogonal to its integer translates.

MRA Requirement 2: The subspaces spanned by the scaling functional low scales are nested within those spanned at higher scales.

As can be seen in the fig.6.1, subspaces containing high- resolution functions must also contain all lower resolution functions. That is

$$V_{-\infty} \subset \cdots V_{-1} \subset V_0 \subset V_1 \subset V_2 \subset \cdots \subset V_{\infty} \qquad \text{---- (6.12)}$$

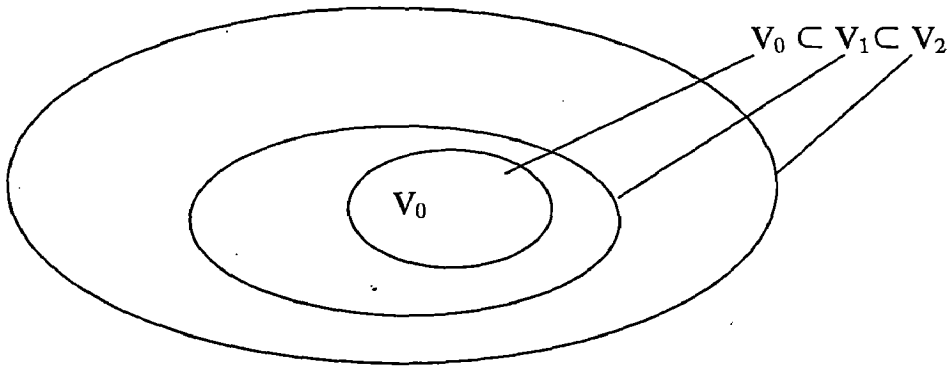

Fig. 6.1 The nested function spaces spanned by a scaling function

Moreover the subspaces satisfy the intuitive condition that if f(x)$\in V_j$,then f(2x)$\in V_{j+1}$.

MRA Requirement 3: The only function that is common to all V_j is f(x)=0.

If we consider the coarsest possible expansion functions (i.e.=- ∞), the only representable function is the function of no information. That is,

$$V_{-\infty} = 0 \qquad \text{---- (6.13)}$$

MRA Requirement 4: Any function can be represented with arbitrary precision.

Though it may not be possible to expand a particular f(x) at an arbitrarily coarse resolution, all measurable, square – integrable functions can be represented in the limit as $j \to \infty$. That is

$$V_{\infty} = \{L^2(R)\} \qquad \text{---- (6.14)}$$

Under these conditions, the expansion functions of subspace V_j can be expressed as a weighted sum of the expansion functions of subspace V_{j+1}. Using Eq.(6.10), we let

$$\phi_{j,k}(x) = \sum_n \alpha_n \phi_{j+1,n}(x)$$

Where the index of summation has been changed ton for clarity. Substituting for $\phi_{j+1,n}(x)$ from Eq.(6.8) and changing variable α_n to $h_\phi(n)$, this becomes

$$\phi_{j,k}(x) = \sum_n h_\phi(n) 2^{(j+1)/2} \phi(2^{j+1}x - n)$$

Since $\phi(x) = \phi_{0,0}(x)$, both j and k can be set to 0 to obtain the simpler non-subscripted expression

$$\phi(x) = \sum_n h_\phi(n) \sqrt{2} \phi(2x - n) \qquad \text{---- (6.15)}$$

The $h_\phi(n)$ coefficients in this recursive equation are called *scaling function coefficients;* h_ϕ is referred as a *scaling vector.* Equation (6.15) is fundamental to multiresloution analysis and is called the *refinement equation,* the *MRA equation,* or the *dilation equation.* It states that the expansion functions of any subspace can be built from double – resolution copies of themselves – that is, from expansion functions of the next higher resolution space. The choice of a reference subspace, V_0, is arbitrary.

6.1.3 Wavelet Functions

Given a scaling function that meets the MRA requirements, we can define a *wavelet function* $\psi(x)$ that, together with its integer translates and binary scalings, spans the difference between any two adjacent scaling subspaces, V_j and V_{j+1}. The situation is illustrated in fig.(6.2). We define the set $\{\psi_{j,k}(x)\}$ of wavelets

$$\psi_{j,k}(x) = 2^{j/2}\psi(2^j x - k) \qquad \text{---- (6.16)}$$

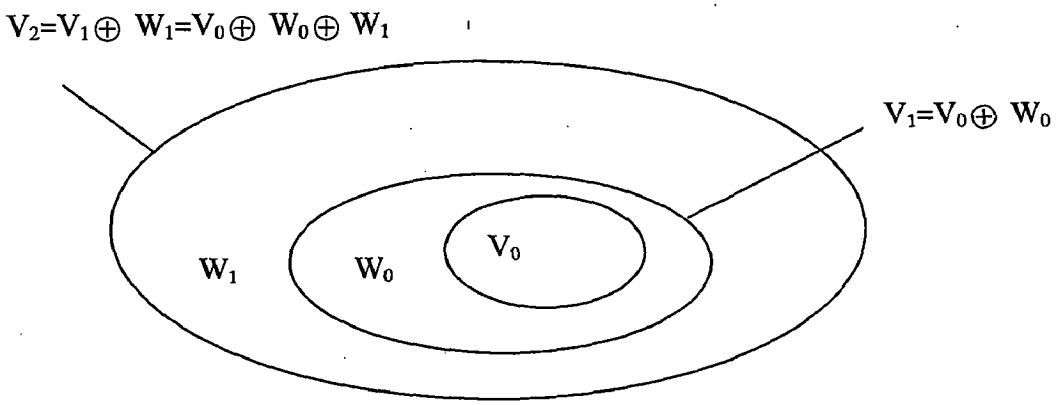

Fig 6.2 The relationship between scaling and wavelet function spaces

Since wavelet spaces reside within the spaces spanned by the next higher resolution scaling functions, any wavelet function – like its scaling function counterpart of Eq.(6.15) can be expressed as weighted sum of shifted, double – resolution scaling functions. That is we can write

$$\psi(\mathrm{x}) = \sum_{\mathrm{n}} h_\psi(\mathrm{n})\sqrt{2}\psi(2\mathrm{x} - \mathrm{n}) \qquad \text{---- (6.17)}$$

Where the $h_\psi(n)$ are called the *wavelet function coefficients and* h_ψ is the *wavelet vector*. Using the condition that wavelets span the orthogonal complement spaces in fig.(6.2), and that integer wavelet translates are orthogonal, it can be shown that $h_\psi(n)$ is related to $h_\phi(n)$ by $\quad h_\psi(n) = (-1)^n h_\phi(1-n)$

6.2. Wavelet Transform in One Dimension

There are several closely related wavelet transformations: the generalized *wavelet expansion*, the *discrete wavelet transform,* the *continuous wavelet transform,* the *Fast Wavelet transform.* Here we are going to discuss only discrete transform and computationally efficient Fast wavelet transform, which play an important role in decomposing and reconstruction of digital mammograms.

6.2.1. The Discrete Wavelet Transform

The wavelet series expansion maps a function of a continuous variable into a sequence of coefficients. If the function being expanded is a sequence of numbers, like samples of a continuous function f(x), the resulting coefficients are called the *discrete wavelet transform* (DWT).

The DWT transform pair is defined as,

$$W_\phi(j_0,k) = \frac{1}{\sqrt{m}} \sum_x f(x)\phi_{j0,k}(x)) \qquad \text{---- (6.18)}$$

$$W_\psi(j_0,k) = \frac{1}{\sqrt{m}} \sum_x f(x)\psi_{j0,k}(x) \qquad \text{---- (6.19)}$$

For $j \geq j_0$ and

$$f(x) = \frac{1}{\sqrt{M}} \sum_x W_\phi(j_0,k)\phi_{j0,k}(x) + \frac{1}{\sqrt{M}} \sum_{j=j_0}^{\infty} \sum_k W_\psi(j,k)\psi_{j,k}(x) \qquad \text{---- (6.20)}$$

Here, f(x), $\phi_{j0,k}(x)$, and $\psi_{j0,k}(x)$ are functions of the discrete variable x=0,1,2... M-1. For example f(x)=f(x_0+ xΔx) for some x_0, Δx, and x = 0,1,2,3... M-1. Normally, we let j_0=0 and select M to be a power of 2 (i.e., M=2^j) so that the summations are performed over x =0,1,2,... M-1, j=0,1,2,... J-1, and k =0,1,2... 2^j -1.

The Equations (6.18) and (6.19) are usually called *approximation* and *detail coefficients,* respectively.

6.2.2 The Fast Wavelet Transform

The *fast wavelet transform* (FWT) is a computationally efficient implementation of the discrete wavelet transform (DWT) that exploits a surprising but fortunate relationship between the coefficients of the DWT at adjacent scales. Also called Mallet's *herringbone algorithm,* the FWT resembles the two – band subband coding scheme.

By considering again, the multiresloution refinement equation,

$$\phi(x) = \sum_n h_\phi(n)\sqrt{2}\phi(2x - n)$$

Scaling x by 2^j, translating it by k, and letting m=2k+n gives

$$\phi(2^j x - k) = \sum_n h_\phi(n)\sqrt{2}\phi(2(2^j x - k) - n)$$
$$= \sum_n h_\phi(m - 2k)\sqrt{2}\phi(2^{j+1} x - m)$$

Note that scaling vector h_ϕ can be thought of as the "weights" used to expand $\phi(2^j x - k)$ as a sum of scale j+1 scaling functions. A similar sequence of operations provides an analogous result for $\psi(2^j x - k)$. That is

$$\psi(2^j x - k) = \sum_n h_\psi(m - 2k)\sqrt{2}\phi(2^{j+1} x - m) \qquad \text{---- (6.21)}$$

Now consider Eq.(6.18) and (6.19), they define the discrete wavelet transform. Substituting Eq.(6.16)- the wavelet defining equation – into Eq.(6.19),we get

$$W_\psi(j,k) = \frac{1}{\sqrt{M}} \sum_k f(x) 2^{j/2} \psi(2^j x - k)$$

Which, upon replacing $\psi(2^j x - k)$ with the right side of Eq.(6.21), becomes

$$W_\psi(j,k) = \frac{1}{\sqrt{M}} \sum_k f(x) 2^{j/2} [\sum_m h_\psi(m - 2k)\sqrt{2}\phi(2^{j+1} x - m)]$$

Interchanging the summand integral and rearranging terms then gives

$$W_\psi(j,k) = \sum_m h_\psi(m - 2k)[\frac{1}{\sqrt{M}} \sum_x f(x) 2^{j+1/2} \phi(2^{j+1} x - m)]$$

Where the bracketed quantity is identical to Eq. (6.18) with j_0 = j+1.

we can therefore write

$$W_\psi(j,k) = \sum_m h_\psi(m - 2k) W_\phi(j+1, m) \qquad \text{----(6.22)}$$

And note that the DWT detail coefficients at scale j are a function of the DWT approximation coefficients at scale j+1. Recognizing Eqs. (6.18) and (6.21) as the starting point of a similar derivation involving the DWT approximation coefficients, we find similarly that

$$W_\phi(j,k) = \sum_m h_\phi(m-2k)W_\phi(j+1,m) \qquad \text{---- (6.23)}$$

Equations (6.22) and (6.23) reveal a remarkable relationship between the DWT coefficients of adjacent scales. We see that both $W_\phi(j,k)$ and $W_\psi(j,k)$, the scale j approximation and the detail coefficients, with the time-reversed scaling and wavelet vectors, $h_\phi(-n)$ and $h_\psi(-n)$, and subsampling the results. Figure (6.3) reduces these operations to block diagram forms. We can therefore write

$$W_\psi(j,k) = h_\psi(-n) * W_\phi(j+1,n)\big|_{n=2k,k\geq 0} \qquad \text{---- (6.24)}$$

And

$$W_\phi(j,k) = h_\phi(-n) * W_\phi(j+1,n)\big|_{n=2k,k\geq 0} \qquad \text{---- (6.25)}$$

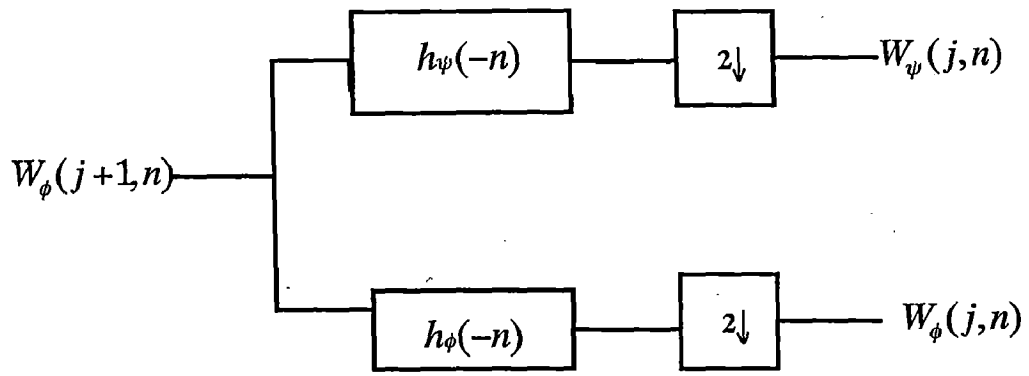

Fig 6.3 An FWT Analysis Bank

Where the convolutions are evaluated at instant n = 2k for k≥0. Evaluating convolutions at nonnegative, even indices is equivalent to filtering and down sampling by 2.

To conclude the development of the FWT, we simply note that the filter bank in Fig.(6.3) can be "iterated " to crate multistage structures for computing DWT coefficients at two or more successive scales. For example, Fig (6.4) shows a two-stage filter bank for generating the coefficients at the two highest scales of the transform.

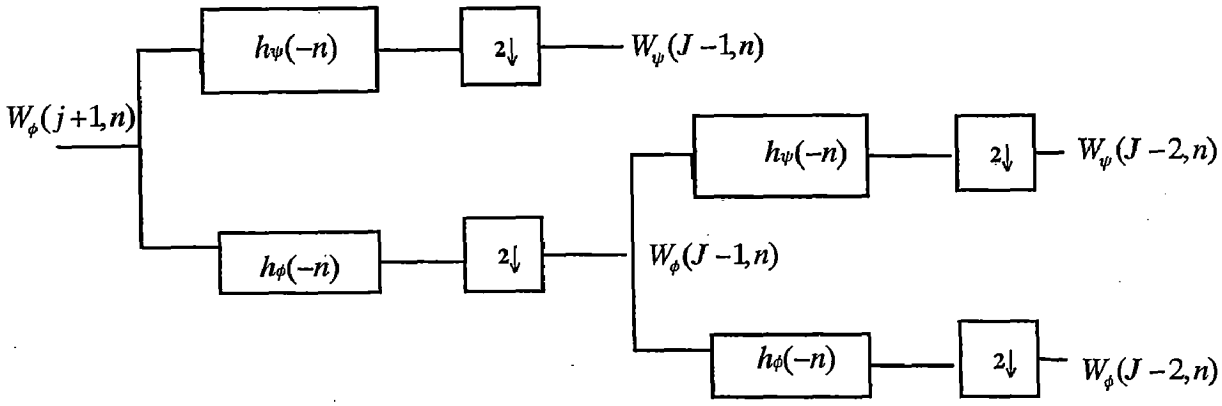

Fig 6.4 A two-scale FWT Analysis Bank

Note that highest scale of coefficients are assumed to be samples of the function itself. That is $W_\phi(J,n)$ = f(n), where J is the highest scale. The filter bank in Fig. (6.4) splits the original function into a lowpass, approximation component, which corresponds to scaling coefficients $W_\phi(J-1,n)$, and a highpass, detail component, which corresponds to scaling coefficients $W_\psi(J-1,n)$.

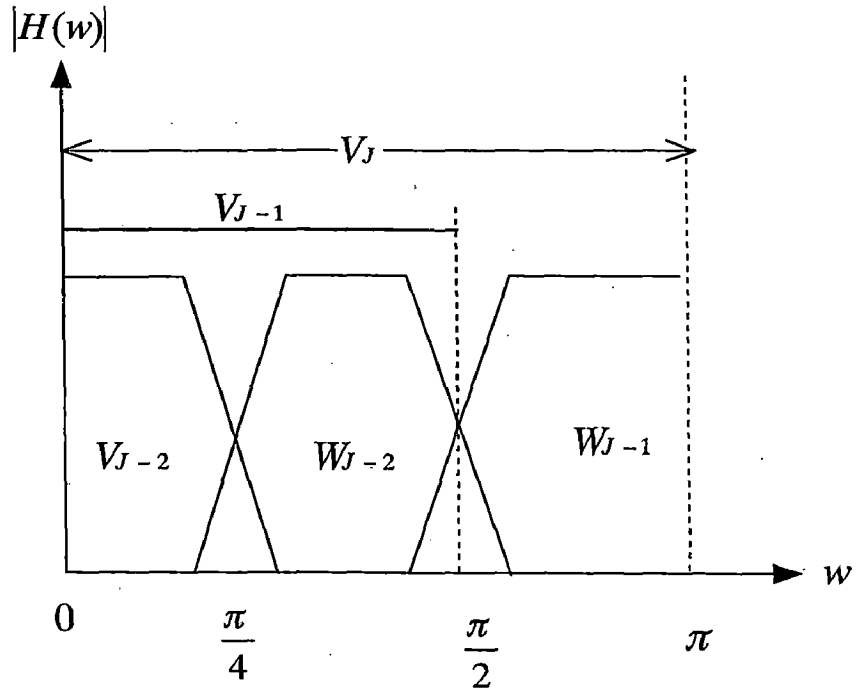

Fig 6.5 Frequency splitting characteristics of fig.(6.4)

This is graphically illustrated in the Fig.(6.5), where scaling space V_J is split into wavelet subspace W_{J-1} and scaling subspace V_{J-1}. The spectrum of the original function is split into two half-band components. The second filter bank in the fig.(6.4) splits the spectrum and subspace V_{J-1}, the lower half –band , into quarter –band subspace W_{J-2} and V_{J-2} - with corresponding DWT coefficients $W_\psi(J-1,n)$ and $W_\phi(J-1,n)$, respectively.

6.3. Wavelet Transforms in Two Dimensions

The one-dimensional transforms (i.e., DWT and FWT) are easily extended to two-dimensional functions like images. In two dimensions, a two-dimensional scaling function, $\phi(x,y)$, and three two-dimensional wavelets $\psi^H(x,y)$, $\psi^V(x,y)$, and $\psi^D(x,y)$, are required. Each is the product of a one-dimensional scaling function ϕ and corresponding wavelet ψ.

Excluding products that produce one dimensional results, like $\phi(x)\psi(x)$, the four remaining products produce the *separable* scaling function

$$\phi(x,y) = \phi(x)\phi(y) \qquad \text{----- (6.26)}$$

And separable, "directional sensitive" wavelets

$$\psi^H(x,y) = \psi(x)\phi(y)$$
$$\psi^V(x,y) = \phi(x)\psi(y)$$
$$\psi^D(x,y) = \psi(x)\psi(y) \qquad \text{(6.27)}$$

These wavelets measure functional variations - intensity or gray –level variation for images – along different directions: ψ^H measures variations along columns (for example, horizontal edges), ψ^V responds to variations along rows (like vertical edges), and ψ^D corresponds to variations along diagonals. The directional sensitivity is a natural consequence of the separability imposed by Eqs.(6.26) and (6.27).

Given separable two-dimensional scaling and wavelet functions, extension of the one-dimensional DWT to two dimensions is straightforward. We first define the scaled and translated basis functions:

$$\phi_{j,m,n}(x,y) = 2^{j/2}\phi(2^j x - m, 2^j y - n) \quad \text{---- (6.28)}$$

$$\psi^i{}_{j,m,n}(x,y) = 2^{j/2}\psi(2^j x - m, 2^j y - n),\ i = \{H,V,D\} \quad \text{---- (6.29)}$$

Where index i identifies the directional wavelet s in Eqs. (6.26) and (6.27). Rather than an exponent, i is a superscript that assumes the values H, V, and D. the discrete wavelet transform of function f(x, y) of size M×N is then

$$W_\phi(j_0,m,n) = \frac{1}{\sqrt{MN}}\sum_{x=0}^{M-1}\sum_{y=0}^{N-1} f(x,y)\phi_{j0,m,n}(x,y) \quad \text{---- (6.30)}$$

$$W_\psi^i(j,m,n) = \frac{1}{\sqrt{MN}}\sum_{x=0}^{M-1}\sum_{y=0}^{N-1} f(x,y)\psi^i{}_{j,m,n}(x,y)\ \ i = \{H,V,D\} \quad \text{---- (6.31)}$$

As in the one-dimensional case, j_0 is an arbitrary starting scale and the $W_\phi(j_0,m,n)$ coefficients define an approximation of f(x, y) at scale j_0. The $W_\psi^i(j,m,n)$ coefficients ad horizontal, vertical, and diagonal details for scales $j \geq j_0$. We normally let $j_0 = 0$ and select N=M= 2^J so that j=0, 1, 2... 2^j -1. Given the W_ϕ and W_ψ^i of Eqs. (6.30) and (6.31), f(x, y) is obtained via the inverse discrete wavelet transform.

$$f(x,y) = \frac{1}{\sqrt{MN}}\sum_m\sum_n W_\phi(j_0,m,n)\phi_{j0,m,n}(x,y) + \frac{1}{\sqrt{MN}}\sum_{i=H,V,D}\sum_{j=j_0}^{\infty} W_\psi^i(j,m,n)\psi^i{}_{j,m,n}(x,y)$$

Like the one-dimensional discrete wavelet transform, the two-dimensional DWT can be implemented using digital filters and downsamplers. With separable two-dimensional scaling and wavelet functions, we simply take the one-dimensional FWT of the rows of f(x, y), followed by the one-dimensional FWT of the resulting columns. Fig.(6.6) shows the process in block diagram form.

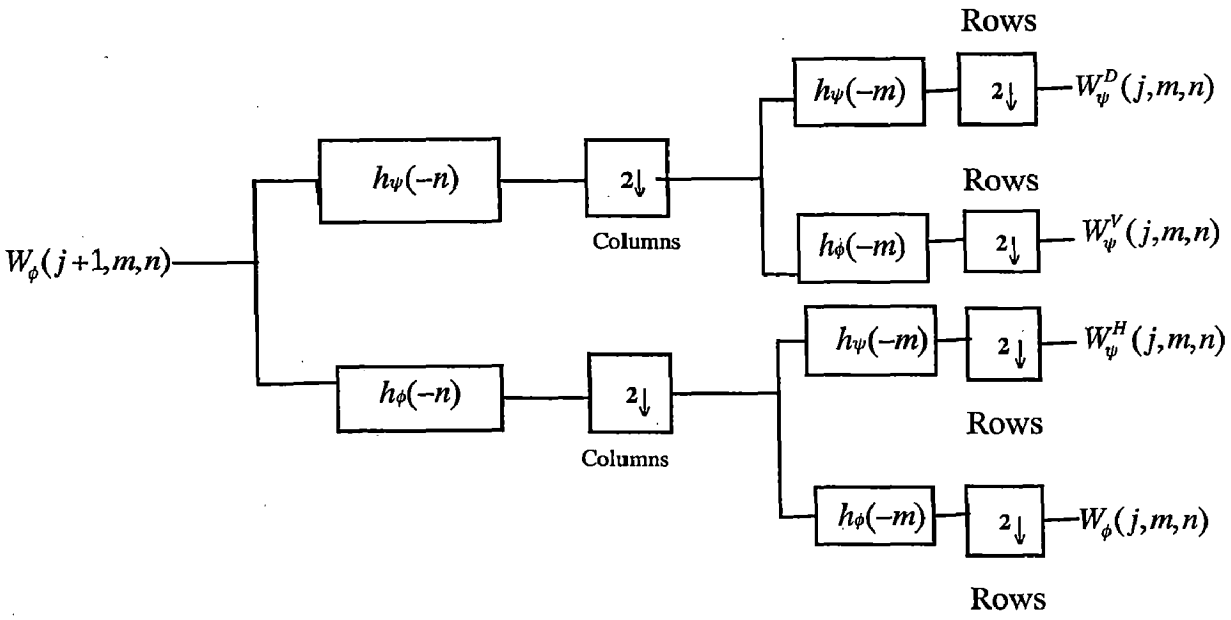

Fig 6.6 The two-dimensional FWT – Analysis Bank

Note that, like its one-dimensional counterpart, the two-dimensional FWT "filters" the scale j+1 approximation coefficients to construct the scale j approximation and detail coefficients. In the two-dimensional case, however, we get three sets of detail coefficients. In the two-dimensional case, however, we get three sets of detail coefficients – the horizontal, vertical and diagonal details.

The single-scale filter bank of Fig.(6.6) can be "iterated" to produce a P scale transform in which scale j=J-1, J-2, ... J-P. As in the one-dimensional case, image f(x, y) is used as the $W_\phi(J,m,n)$ input. Convolving its rows with $h_\phi(-n)$ and $h_\psi(-n)$ and downsampling its columns, we get two subimages whose horizontal resolutions are reduced by a factor of 2. The highpass or detail component characterizes the image's high-frequency information with vertical orientation; the lowpass, approximation component contains its low-frequency, vertical information.

Both subimages are then filtered column wise and down sampled to yield four quarter-size output subimages- $W_\phi, W_\psi^H, W_\psi^V$, and W_ψ^D.

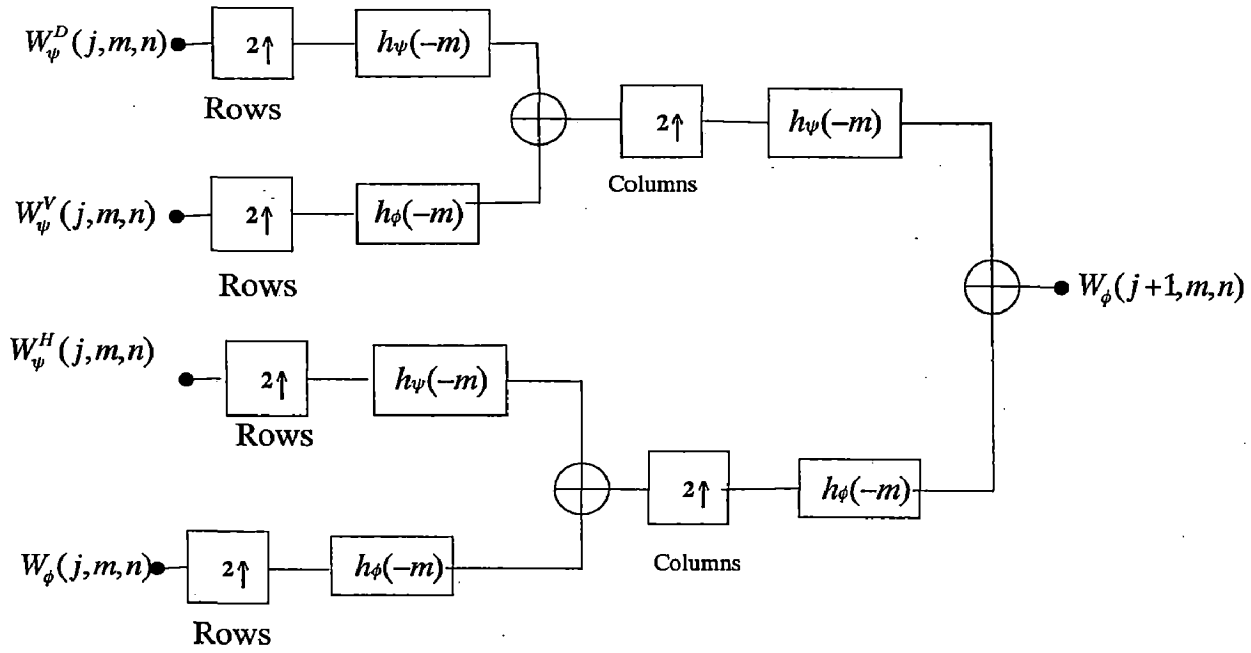

Fig 6.7 The FWT two-dimensional Synthesis Bank

Figure (6.7) shows the synthesis filter bank that reverses the process described above. As would be expected, the reconstruction algorithm is similar to the one-dimensional case. At each iteration, four scale j approximation and detail subimages are upsampled and convolved with two one-dimensional filters- one operating on the subimages columns and the other on its rows. Addition of the results yields the scale j+1 approximation, and the process is repeated until the original mage is reconstructed.

6.4 Multiscale Decomposition & Reconstruction System

Screening of digital mammograms for clusters of microcalcifications indicating malignancy can be facilitated by a system capable of extracting spurious spots in digital mammograms regardless of a system proposed to perform this task by exploiting the frequency selectivity of wavelet-based subband image decomposition.

The proposed system has been shown below.

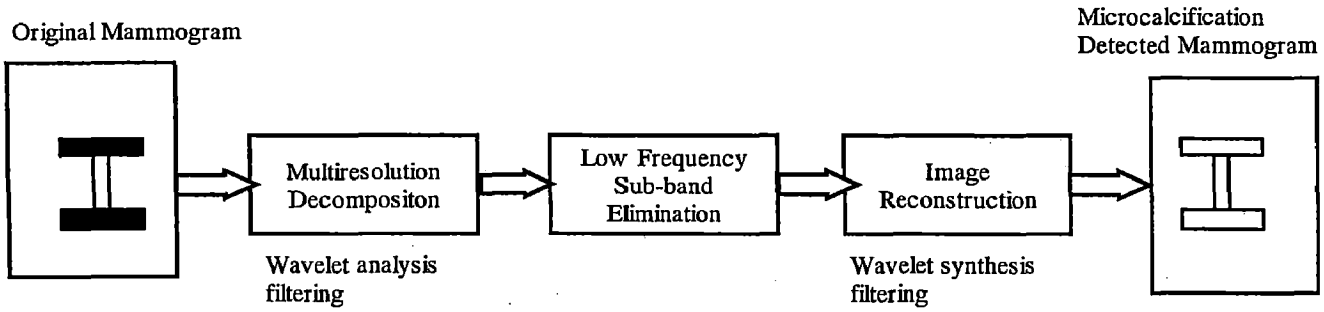

Fig.6.8 The proposed system in operation

The input to the system is a digital mammogram, and the output is a mammogram with detected microcalcifications.

The system proposed for microcalcification detection is based on the hypothesis that the microcalcifications present in mammograms can be preserved under a transform which can localize the signal characteristics in the original and the transform domain. In a time signal the harmonic frequency components are present but they are hidden, whereas it its frequency spectrum the time information is hidden. Therefore, transforms with basis functions other than the complex sinusoids must be used. In addition, these basis functions must be able to localize the signal in both spatial and frequency domains. A suitable transform that satisfies the above requirement is the wavelet transform. The wavelet transform uses basis functions that can dilate in scale and translate in position according to the signal characteristics.

Given that the microcalcifications correspond to high-frequency components of the image spectrum and wavelets can localize the signal characteristics in both frequency and scale, our hypothesis is that the resolution and scale of the

microcalcifications in the spatial domain can be preserved if we use wavelet filters to decompose the mammogram into different frequency sub-bands. According to this hypothesis, microcalcifications can be extracted from mammograms by suppressing the subband of the wavelet-decomposed image that carries the lowest frequencies and contains smooth (background) information, before the reconstruction of the image.

The proposed system is described in the block diagram shown in Fig.6.8. The original mammogram is decomposed into a set of decomposed images of different resolution and frequency content. The decomposition is based on wavelet analysis filtering and downsampling along the rows and columns of the image. Here the ROI of the digital mammogram "mdb209" from MIAS Image Database has been decomposed into 3 decomposition levels using "db4" mother wavelet is shown below.

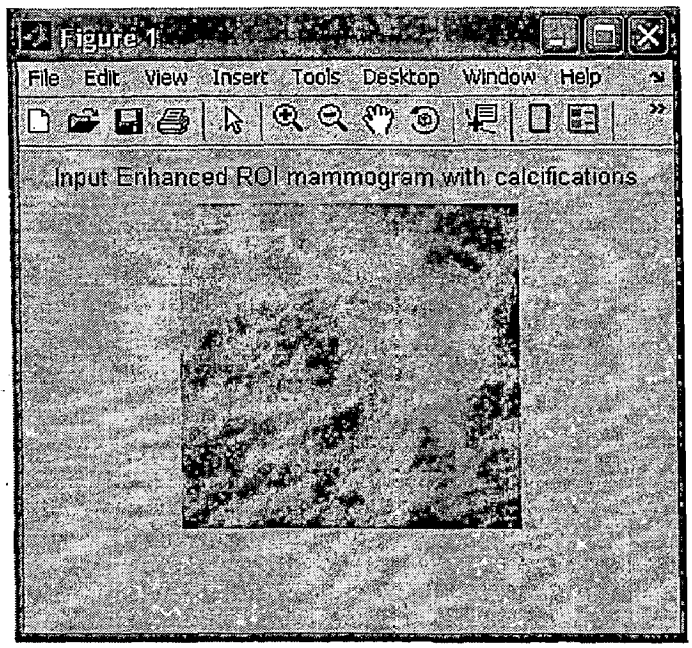

Fig.6.9(a) Input ROI of the mammogram with Calcifications

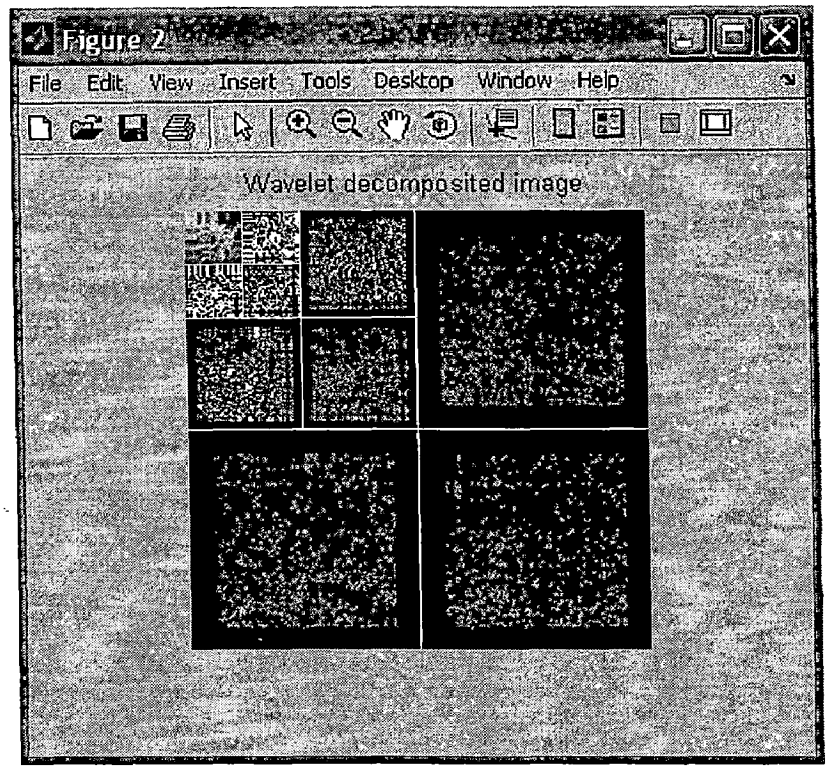

Fig 6.9(b) Wavelet Decomposed image.

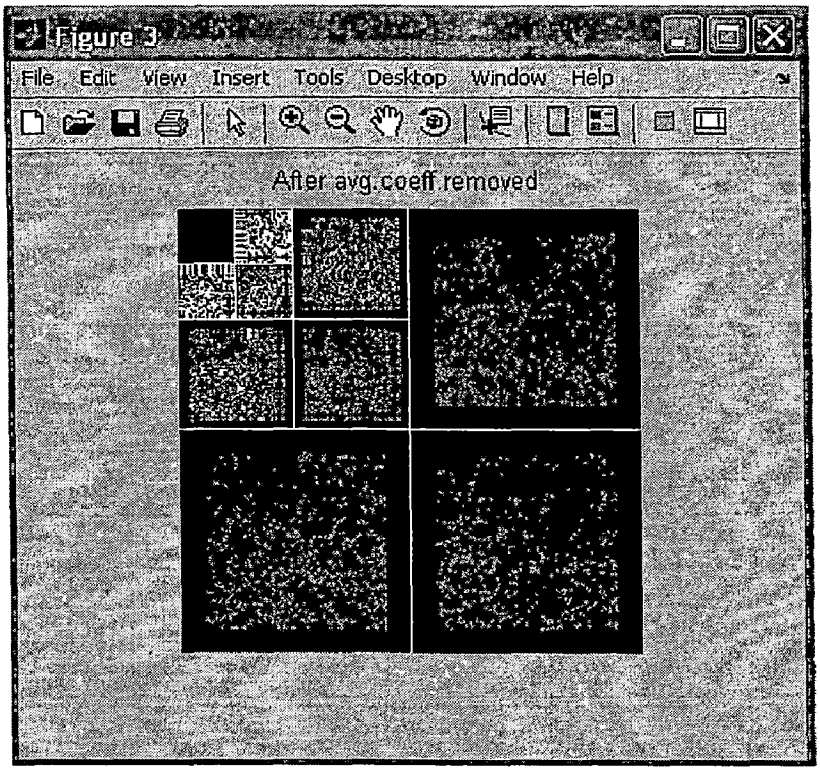

Fig.6.9(c) After removing Avg.image

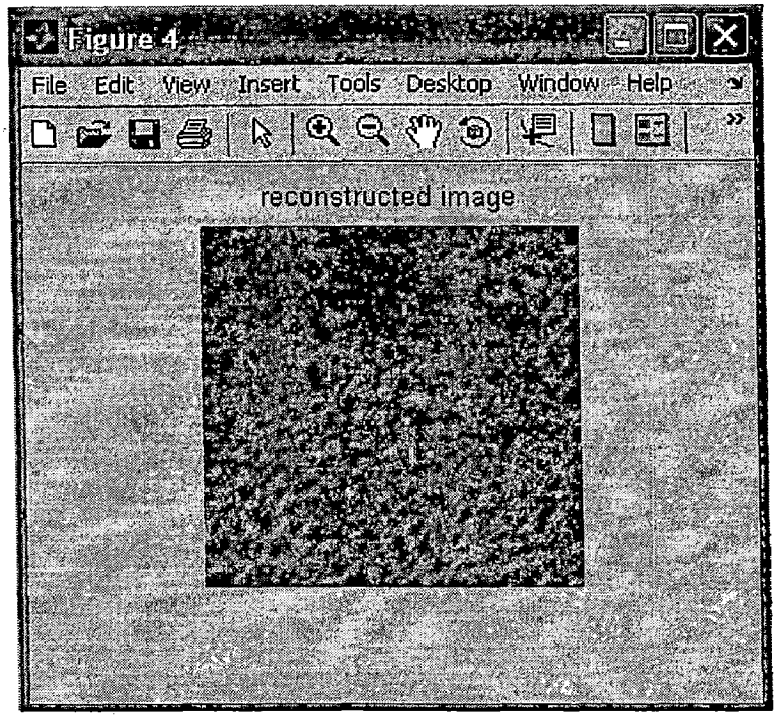

Fig. 6.9(d) Reconstructed Image

The upper-left subband at decomposition level 3 shown in Fig.6.9 (b) contains the background intensity of the original image and, thus, carries the lowest frequencies of the image spectrum. The microcalcifications, which correspond to highest frequencies, are carried by the other sub-bands. The wavelet coefficients are accomplished by setting the wavelet coefficients of the upper-left subband to zero in order to suppress the image background information before reconstruction of the image. The reconstructed image is expected to contain only high-frequency components, including the microcalcifications. The final images are obtained using subband reconstruction, which is the inverse operator of subband decomposition. The reconstruction consists of wavelet synthesis filtering and upsampling along the rows and columns of the image.

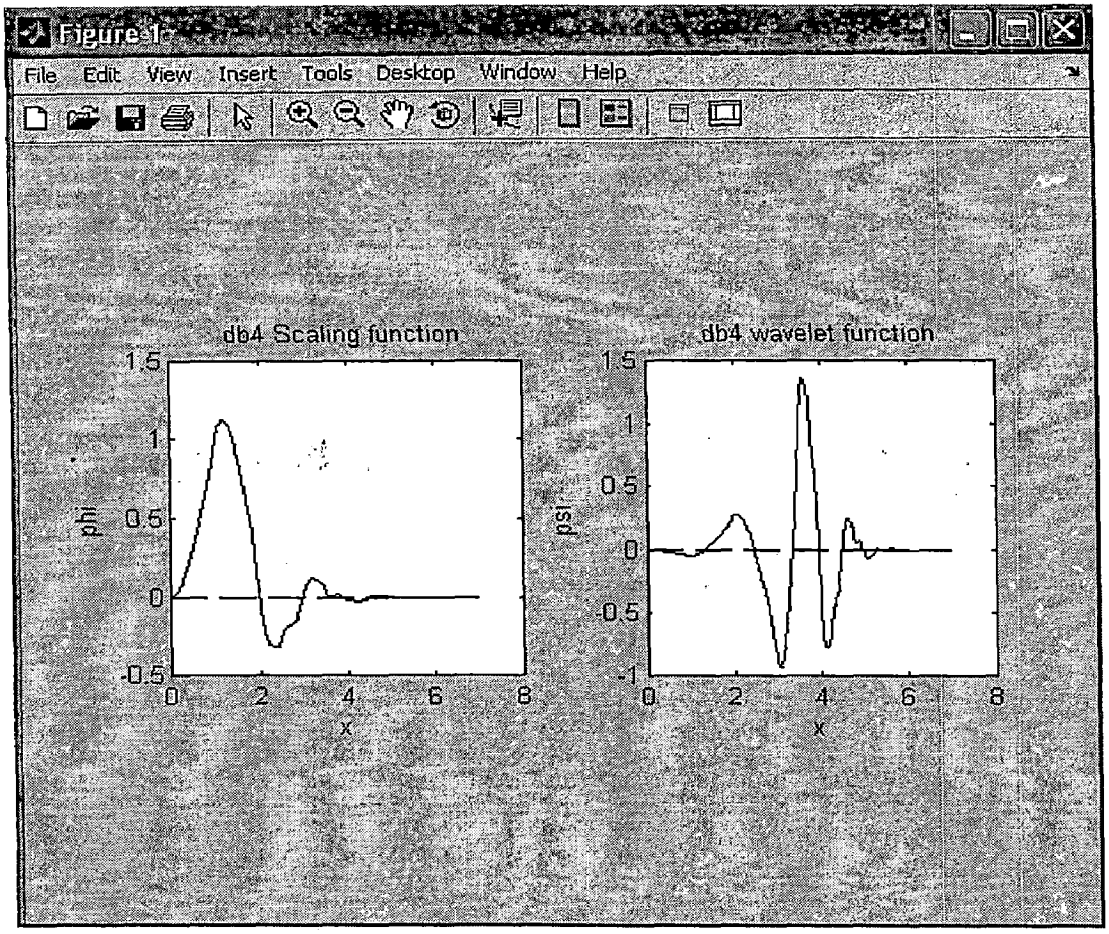

Fig.6.10 Scaling and wavelet function of type 'db4'

In the "wavelet analysis filtering" and "wavelet synthesis filtering" stages, the so-called "maximally flat" wavelet filters constructed by Daubeches [10]. These wavelets are compactly supported if they have finite support with maximum number of vanishing moments for their support width. Compact support improves the time resolution of wavelets. Regularity relates to differentiability. The Daubeches wavelet and scaling functions have been shown in the Fig. (6.10)

6.5 Otsu's thresholding Technique

As the reconstructed image having along with the microcalcifications, it consists of some other unwanted information. So there is a need for thresholding the image, so that the output binary image will consist only microcalcifications.

In this work, an automatic global threshold is being used, which is produced by the Otsu's method. Otsu's method is based on selecting the lowest point between the two peaks in the histogram of the image.

Here some terminology is given in conjunction with the Otsu's method.

Frequency: $$w = \sum_{i=0}^{T} P(i)$$

Mean: $$\mu = \sum_{i=0}^{T} P(i)/w$$

Total Variance: $$\delta_t^2 = \sum_{i=0}^{T} (i-\mu)^2 P(i)$$

Where P(i) = n_i/N, n_i = number of pixels in level i, and N = total number of pixels in the image.

Between-class Variance: The variation of the mean values for each class from the overall intensity mean of all pixels is defined as between-classes variance.

$$\delta_b^2 = w_0(\mu_0 - \mu_t)^2 + w_1(\mu_1 - \mu_t)^2$$

Substituting $\mu_t = w_0\mu_0 + w_1w_1$,

We get $$\delta_b^2 = w_0w_1(\mu_1 - \mu_0)^2$$

w_0, w_1, μ_0, μ_1 stands for the frequencies and mean values of two classes, respectively.

The criterion function involves *between-classes* variance to the total variance is defined as $$\eta = \delta_b^2 / \delta_t^2$$

All possible thresholds are evaluated in this way, and the one that maximizes η is chosen as the optimal threshold.

The threshold generated by the Otsu's method is taken as a reference threshold, and a series of thresholded images have been generated by small incremental in steps of 0.05 of the reference threshold. It is found that at a variance of 0.3 to the reference threshold will reasonably gives the binary image which includes the microcalcifications. The final thresholded image which consists of microcalcifications is being produced in the next section. And this result is to be verified clinically by a radiologist.

RESULTS & DISCUSSIONS

This chapter will elobarates the results that have been obtained in the various stages of the thesis. The results can be broadly classified into two parts, one is related to processing of the mammograms i.e., enhancement of the mammograms and the second one is related to extraction of microcalcifications from the mammograms.

Details of Image Database

In this dissertation work, the Mammographic Image Analysis Society (MIAS) Mini Mammographic Database [8], which contains 322 mammograms including normal, mass, and microcalcification cases, have been used. The image size in the Mini Mammographic database has been clipped and padded to become 1024×1024 pixels whose spatial resolution is 200μm and dynamic range is 8-bit. In this work, the microcalcifications of 0.05 to 1.0 mm in diameter are of interest, which corresponding to one to five pixels in diameter.

Enhancement of Mammograms

The mammograms have been enhanced by four different methods. Out of them two are classical and well established methods, namely, Histogram Equalization and Contrast Stretching, and other two methods are recently developed and they are Morphological Enhancement methods based on top-hat and bottom-hat algorithms, and the second one is Adaptive Histogram Equalization.

All the above mentioned methods have been quantitatively compared based on recently proposed parameters like Distance Separation Measure (DSM), Target to Background Contrast Enhancement Measurement based on standard deviation (TBC_s), and Target to Background Contrast Enhancement Measurement based on Entropy (TBC_e). A unique quantitative measure which includes all the above measuring parameters is being devised and it is named as D. Based on this D value different enhancement techniques have been compared.

Here some of the graphs related to different enhancement techniques have been shown. The computational procedure which is developed based on the above quantitative measures will gives out a best enhanced image out of all other available enhanced images. The minimum the value of D, the better the enhancement method.

Image mdb209:

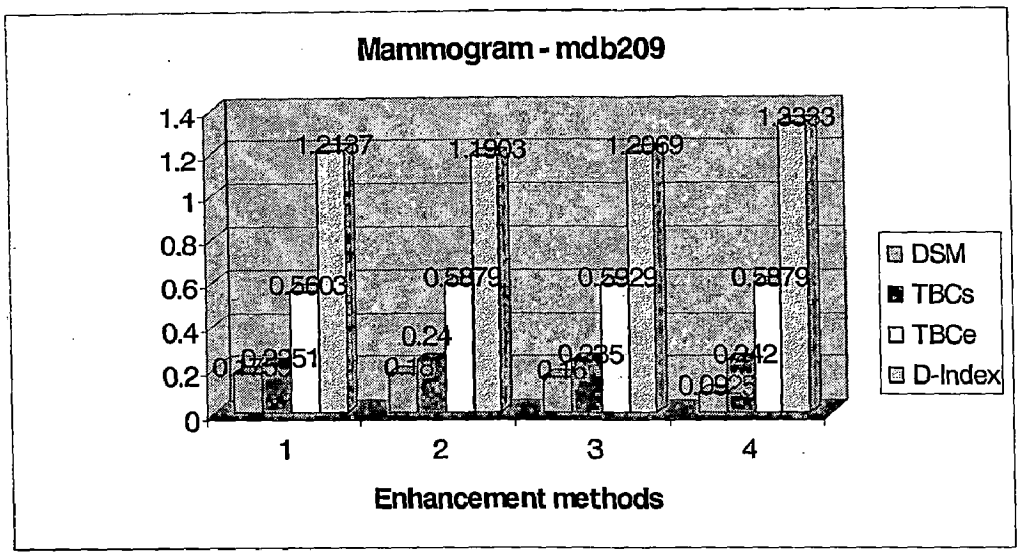

Image mdb213:

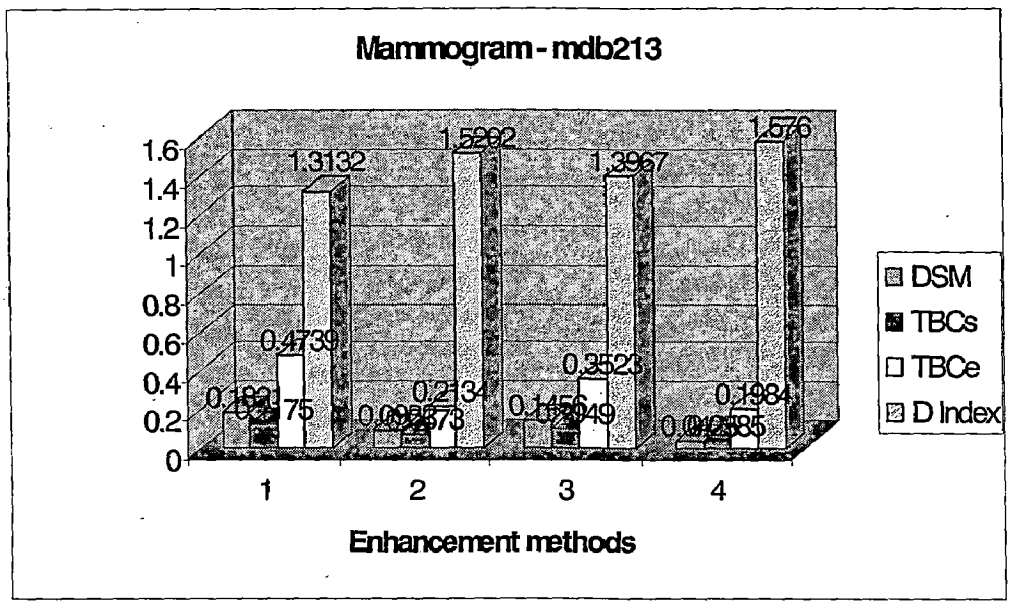

Image mdb233:

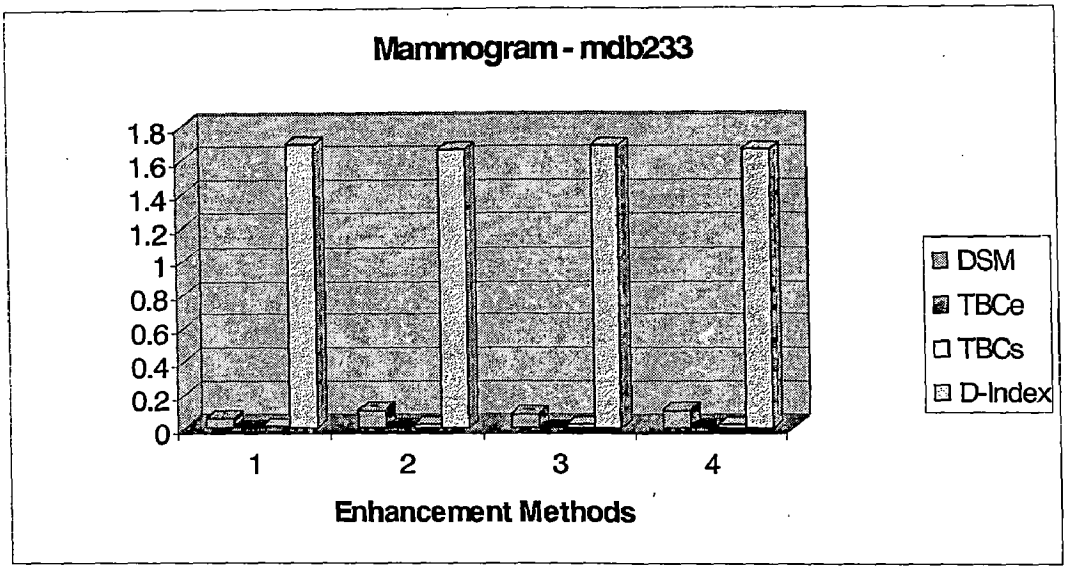

Image mdb241:

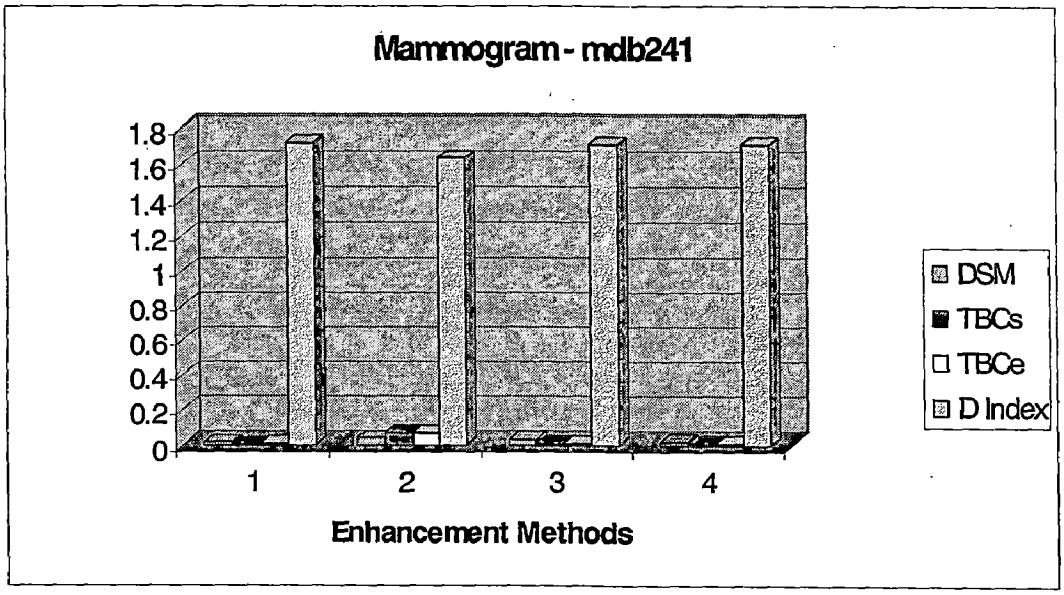

Image mdb249:

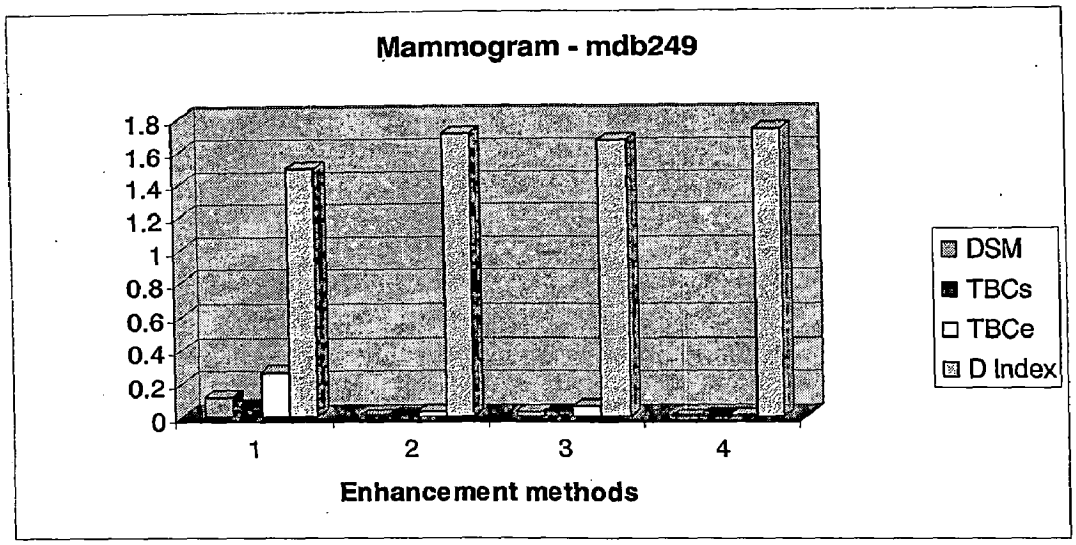

The enhancement methods are

1. Histogram Equalization

2. Adaptive Histogram Equalization

3. Contrast Stretching

4. Morphological Enhancement

In the below figure, D index has been plotted for various images in the database.

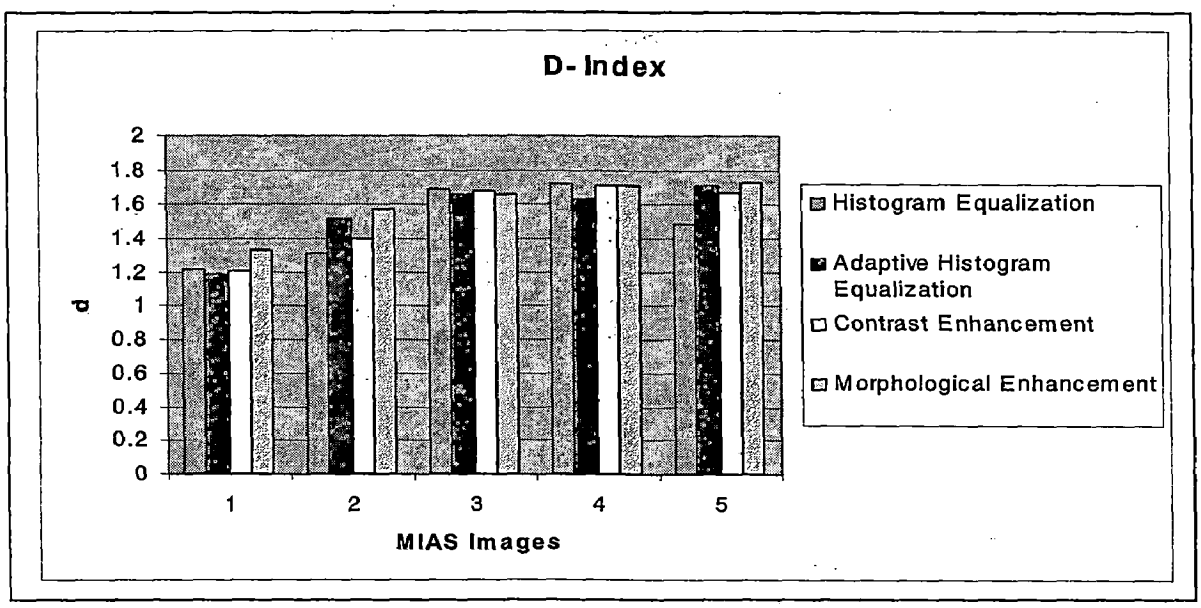

From the above graphs, the conclusion can be, there is no unique method of enhancement technique for all the mammograms. so the quantitative measures help us select the best suited image enhancement on a per mammogram basis, which improves the quality of segmentation much better than using the same enhancement methods for all mammograms.

Detection of Microcalcifications

Mammograms are among the most difficult of radiological images to interpret; in particular, microcalcification visual assessment turns out to be an actual challenging task. As the microcalcifications vary in size from smaller than 0.1mm to 1 mm in diameter and a radiologist must carefully examine the mammogram with a magnifier to locate calcifications which may be embedded in dense tissue. Size, shape, and radiographic density are the most important factors on analyzing individual calcifications.

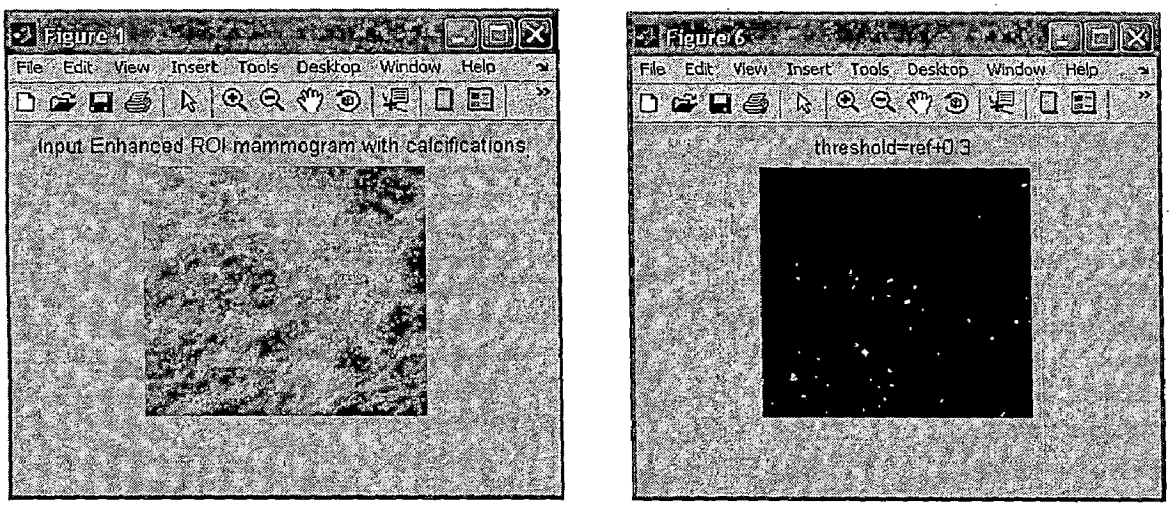

Fig.7.1 Mammogram with detected microcalcifications

Wavelet analysis is an extremely powerful data representation method that allows for the separation of images into frequency bands without affecting the spatial locality. Thus, information concerning localized high-frequency signals such as microcalcifications can be extracted effectively. In this work, the ROI of the mammograms have been decomposed into different levels, and the low-frequency information, which do not contain microcalcifications have been removed. And it is followed by thresholding, which will give the binary image, consists of microcalcifications. Here the original ROI and detected microcalcifications have been shown.

In the preprocessing stage of the mammographic image analysis, various image enhancement techniques have been compared, and the best enhanced image has been further processed and it can be verified that, no unique enhancement method is fit for all the mammographic images.

The microcalcification detection method is based on a multi-scale representation of the mammographic image. Motivation for adapting a multi-scale representation stems form the fact that microcalcifications reveal some evident features at some specific scale, while being invisible at other scale. Differently from other methods [3], microcalcification detection is thoroughly performed on the transformed image. The reference threshold is automatically determined using Otsu's method and around variance of 0.3 from the reference threshold, microcalcifications have been detected.

Scope of the future work

Still there is no universal method is there for detection of calcifications, especially in determining the threshold, a lot of work should be done in that area.

After successful detection of microcalcifications, they have to be classified into two groups. One is Benign, and the other one is malignant calcifications. So ample of scope for research is there in the design of the classifier and successful classification.

[1] http://www.dep.iarc.fr/

[2] http://www.canceratlasindia.org

[3] Giuseppe Boccignone, Angelo Chianese, Antonio Picariello, "Computer aided Detection of microcalcifications in digital mammograms", PERGAMON, Computers in Biology and Medicine 30:267-286, 2000

[4] R.N. Strickland and H.I. Hahn, "Wavelet Transform for Detecting Microcalcification in Mammograms," IEEE Trans. Med. Imag. Vol 15, No.2, pp 218-229, April 1996.

[5] M.N.Gurcan, Y. Yardimci, A.E. Cetin and R.Ansari, "Automated Detection and Enhancement of Microcalcification on Digital Mammograms using Wavelet Transform Techniques," Dept. of Radiology, Univ. of Chicago, 1997.

[6] R.N.Strickland, H.I. Han, "Wavelet Transform for Detecting Microcalcifications in Mammograms," IEEE Tran. Med. Imag., Vol.15, No.2, pp 218-229, 1996

[7] Robin N. Stricklnad, Hee Hahn, "Wavelet Transforms for Detection Microcalcifications in Mammograms," IEEE Transactions on Medical Imaging., Vol 15, No. 2, Apr. 1996.

[8] J. Suckling et al (1994) "The Mammographic Image Analysis Society Digital Mammogram Database" Exerpta Medica. International Congress Series 1069 pp375-378 [http://peipa.essex.ac.uk/ipa/pix/mias/]

[9] Sang Hee Nam, Jun Young Choi "A Method of Image Enhancement and Fractal Dimension for Detection of Microcalcifications in Mammogram," Proc. Of 20th Annual International Conference of the IEEE Engg. In Medicine and Biology Society, Vol.20, No.2, 1998

[10] Ted C. Wang and Nicolaos B. Karayiannis, "Detection of Microcalcifications in Digital Mammograms Using Wavelets," IEEE Trans.Med.Imag., vol. 17 No.4, Aug 1998.

[11] Kim, J.K., Park J.M., Song S. S., and Park H. W. "Adaptive Mammogram Image Enhancement Using First Derivative and Local Statistics," IEEE Trans. Med. Imag. Vol. 16, No.5, pp. 495-502, 1997.

[12] K.S. Woods Automated Image Analysis Techniques for Digital Mammography, Ph.D Thesis, University of Maryland, Maryland, 1994.

[13] D.H. Davies, D.R. Dance, "Automatic computer detection of clustered microcalcifications in digital mammograms", Physics in Medicine and Biology 35 (8) (1990) 1111-1118.

[14] J. Dengler, S. Behrens, J.F. Desaga, Segmentation of microcalcifications in mammograms, IEEE Transactions on Medical Imaging 12 (4) (1993) 634-642.

[15] Laine A and Song S, "Wavelet processing techniques for digital Mammography",
Proc of the SPIE/IS&T SYMPOSIUM ON Electronic Imaging Science and Technology, 1993.

[16] R.M. Rao and Ajit S.Bopardikar, "Wavelet Transforms- Introduction to Theory and Applications" Pearson Education, 2002

[17] Robi Polikar, "Wavelet Tutorials", Rowan University, 2004

[18] W.Marrow, R. Paranjape, R.Rangayyan, and J.Desautels, "Region based contrast enhancement of mammograms," IEEE Trans. Med.Imag., vol. 11. pp, 392-406, June 1992.

[19] Mallat S., "Multifrequency channel decompositions of images and wavelet models," IEEE Trans. Acoust. Speech, Signal Proc 37:2091-2110, 1989

[20] K.S. Woods, Automated Image Analysis Techniques for Digital Mammography, Ph.D Thesis, University of Maryland, Maryland, 1994.

[21] Rafael C.Gonzalez, Richard E.Woods, Steven L.Eddins "Digital Image Processing using MATLAB" pp.366-370 Pearson Education, 2004.

22] K.J. Bovis and S. Singh "Enhancement technique evaluation using quantitative neasures" in Proc. 5th Int. Workshop Digital Mammography, Toronto,Canada,2000, p. 547-553

[23] M.Singh, S.Singh, and D.Partridge, "A knowledge based framework for image enhancement in aviation security," IEEE Trans.Syst.,Man, cybern. B., vol. 34, no. 6, pp.2354-2365, Dec. 2004.

[24] Sameer Singh, Keir Bovis "An Evaluation of Contrast Enhancement Techniques for Mammographic Breast Masses," IEEE Trans. on Information Technology in Biomedicine Vol.9, No.1, March 2005.

[25] Rafael C.Gonzalez, R.E.Woods, "Digital Image Processing", second edition, Pearson Education, pp 349-386,2004